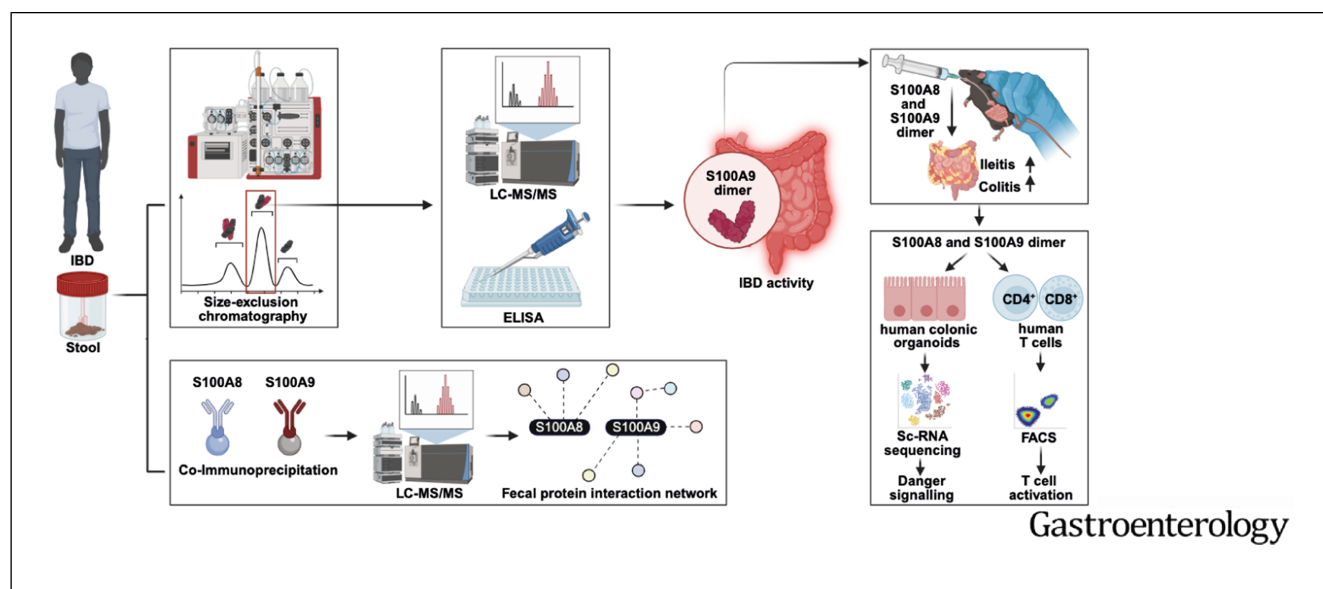


Fecal Detection of Calprotectin Subunits Links Inflammatory Bowel Disease Activity With Chronicity of Intestinal Inflammation

Almina Jukic,¹ Richard Hilbe,² Luis Zundel,¹ Peter Willeit,^{3,4} Klaus Faserl,⁵ Christina Plattner,⁶ Andreas Zollner,¹ Moritz Meyer,¹ Kerstin Siegmund,⁷ Victoria Klepsch,⁷ Valentin Marteau,⁶ Arnau Vich Vila,⁸ Julian Schwärzler,¹ Kathrin Vouk,¹ Anna Kozsar,¹ Dietmar Rieder,^{6,9} Amos Weichberger,^{10,11} Bettina Sarg,⁵ Felix Grabherr,¹ Lisa Mayr,¹ Patrizia Moser,¹² Niloofar Nemati,⁶ Sabine Scholl-Bürgi,¹³ Daniela Karall,¹³ Georg F. Vogel,^{13,14} Lina Welz,¹⁰ Denise Aldrian,¹³ Robert Koch,¹ Alexandra Pfister,¹ Qitao Ran,¹⁵ Arthur Kaser,¹⁶ Richard S. Blumberg,¹⁷ Ivan Tancevski,² Felix Sommer,¹⁰ Petra Bacher,^{10,11} Stefan Schreiber,¹⁰ Philip Rosenstiel,¹⁰ Konrad Aden,¹⁰ Gottfried Baier,⁷ Latifa Bakiri,¹⁸ Thomas Müller,¹³ Günter Weiss,² TRR241 IBDome Consortium, Rinse K. Weersma,⁸ Zlatko Trajanoski,⁶ Erwin F. Wagner,^{18,19} Herbert Tilg,¹ and Timon E. Adolph¹

¹Department of Internal Medicine I, Gastroenterology, Hepatology, Endocrinology & Metabolism, Medical University of Innsbruck, Innsbruck, Austria; ²Department of Internal Medicine II, Infectious Diseases, Immunology, Rheumatology, Pneumology, Medical University of Innsbruck, Innsbruck, Austria; ³Institute of Clinical Epidemiology, Public Health, Health Economics, Medical Statistics and Informatics, Medical University of Innsbruck, Innsbruck, Austria; ⁴Department of Public Health and Primary Care, University of Cambridge, Cambridge, United Kingdom; ⁵Biocenter, Protein Core Facility, Institute of Medical Biochemistry, Medical University of Innsbruck, Innsbruck, Austria; ⁶Biocenter, Institute of Bioinformatics, Medical University of Innsbruck, Innsbruck, Austria; ⁷Institute of Cell Genetics, Medical University of Innsbruck, Innsbruck, Austria; ⁸Department of Gastroenterology and Hepatology, University of Groningen and University Medical Center of Groningen, Groningen, the Netherlands; ⁹Biocenter, Bioinformatics Core Facility, Medical University of Innsbruck, Innsbruck, Austria; ¹⁰Institute of Clinical Molecular Biology, Christian Albrecht University Kiel and Schleswig-Holstein University Hospital, Kiel, Germany; ¹¹Institute of Immunology, Christian Albrecht University Kiel and Schleswig-Holstein University Hospital, Kiel, Germany; ¹²INNPATh, Innsbruck Medical University Hospital, Innsbruck, Austria; ¹³Department of Pediatrics I, Medical University of Innsbruck, Innsbruck, Austria; ¹⁴Institute of Cell Biology, Medical University of Innsbruck, Innsbruck, Austria; ¹⁵Department of Cell Systems and Anatomy, University of Texas Health San Antonio, San Antonio, Texas; ¹⁶Cambridge Institute of Therapeutic Immunology and Infectious Disease, Department of Medicine, University of Cambridge, Cambridge, United Kingdom; ¹⁷Gastroenterology Division, Department of Medicine, Brigham and Women's Hospital, Harvard Medical School, Boston, Massachusetts; ¹⁸Department of Laboratory Medicine, Medical University of Vienna, Vienna, Austria; and ¹⁹Department of Dermatology, Medical University of Vienna, Vienna, Austria



BACKGROUND & AIMS: Quantification of the human S100A8/S100A9 tetrameric protein complex in stool, referred to as fecal calprotectin, is an extensively validated biomarker supporting the diagnosis and management of gastrointestinal diseases. Here, we studied the quaternary protein structures (termed configuration) of S100A8 and S100A9 and their biological function in inflammatory bowel diseases (IBD). **METHODS:** We dissected fecal S100A8 and S100A9 configurations in patients with IBD by size-exclusion chromatography coupled with tandem mass spectrometry and systematically defined human S100A8 and S100A9 homodimer functions compared with the calprotectin heterotetramer (CP) in the intestine of mice and in human epithelium and T cells. Moreover, we report a protein interaction network of fecal S100A8 and S100A9 in IBD. **RESULTS:** Stool from patients with active IBD contained abundant S100A8 and S100A9 dimers besides CP. Fecal S100A9 detection associated with clinical and endoscopic disease activity in IBD patients with low CP concentration. Oral exposure to human recombinant S100A8 and S100A9 homodimers, but not to CP, worsened intestinal inflammation in toxic and genetic mouse models. Functional profiling revealed that human S100A8 and S100A9 homodimers enhanced activation of cluster of differentiation 4⁺ and 8⁺ T cells, which promoted experimental colitis. In turn, genetic inactivation of *S100a9* protected against experimental enteritis and colitis, and pharmacologic inhibition of S100A9 ameliorated chronic colitis. **CONCLUSIONS:** Collectively, this study links the detection of fecal S100A9 dimers with clinical and endoscopic disease activity in IBD and identifies inflammatory actions of S100A8 and S100A9 homodimers in the intestine. Our findings pave the way for novel diagnostic and therapeutic approaches in patients with inflammatory diseases of the intestine.

Keywords: Calprotectin; S100A8; S100A9; Inflammatory Bowel Diseases; Crohn's Disease; Ulcerative Colitis; Intestinal Inflammation.

Inflammatory bowel diseases (IBD), such as Crohn's disease (CD) and ulcerative colitis (UC), are complex immune-mediated inflammatory conditions of the intestine and extraintestinal tissues with increasing incidence and prevalence across the globe during recent decades.^{1,2} The underlying cause of chronic unresolved intestinal inflammation remains enigmatic for most patients with IBD, and host-related mediators of disease chronicity are poorly defined.^{3,4} Quantification of calprotectin (CP) in stool, determined by enzyme-linked immunosorbent assay (ELISA), is a rapid and noninvasive technique that allows the assessment of inflammatory diseases of the intestine, for example, the evaluation of suspected or established IBD.⁵ More specifically, fecal CP indicates an inflammatory condition in the intestine with high sensitivity irrespective of the underlying cause, and—in the case of IBD—mirrors endoscopic disease activity.⁵ Fecal CP concentration >150 µg/g suggests active disease in patients with IBD, and normalization of fecal CP concentration (to 100–250 µg/g fecal CP) is an intermediate treatment goal in IBD.^{5,6} By contrast, the biological function of CP in the human intestine

WHAT YOU NEED TO KNOW

BACKGROUND AND CONTEXT

Fecal calprotectin serves as an inflammatory biomarker in patients with inflammatory bowel disease and is composed of a heterotetrameric protein complex of S100A8 and S100A9 dimers. The quaternary structure (protein configuration) of S100A8 and S100A9 and related biological functions are unknown in the intestine.

NEW FINDINGS

We reveal the presence of S100A8 and S100A9 dimers, besides calprotectin, in stool from patients with active inflammatory bowel disease and identify human S100A8 and S100A9 homodimers, but not calprotectin, as drivers of enteritis and colitis in mice.

LIMITATIONS

Large controlled trials with endoscopy endpoints are warranted to establish diagnostic or therapeutic value in targeting S100A8 and S100A9 in inflammatory bowel disease.

CLINICAL RESEARCH RELEVANCE

Our study opens up new perspectives for S100A8 and S100A9 dimer detection as biomarkers of inflammatory diseases in the intestine. Pharmacologic targeting of S100A8 or S100A9 dimers may be exploited to treat inflammatory bowel diseases in the future.

BASIC RESEARCH RELEVANCE

Human S100A8 and S100A9 homodimers, but not calprotectin, promote chronicity of intestinal inflammation by pleiotropic mechanisms. These insights can be leveraged to treat inflammatory disorders of the intestine.

is poorly understood, and experimental studies in colitis models have demonstrated conflicting biological effects.^{6–9}

CP is an evolutionary conserved protein complex with ion-chelating properties. It is composed of S100A8 and S100A9 proteins that share high structural homology.¹⁰ In the intestine, S100A8 and S100A9 are almost exclusively expressed by myeloid cells such as neutrophils and macrophages. Upon danger signaling during infection or inflammation, S100A8 and S100A9 are passively released by dying cells⁶ or secreted by E-selectin-induced gasdermin D pores.¹¹ In the extracellular space, heterotetramerization of S100A8 and S100A9 into CP is facilitated by ion availability (eg, calcium or zinc).¹²

It has been postulated that distinct quaternary protein structures (from now on referred to as *configurations*) of

Abbreviations used in this paper: CD#, cluster of differentiation; CD, Crohn's disease; CP, calprotectin; DSS, dextran sodium sulfate; ELISA, enzyme-linked immunosorbent assay; GPX4, glutathione peroxidase 4; IBD, inflammatory bowel disease; IEC, intestinal epithelial cells; LC, liquid chromatography; MS/MS, tandem mass spectrometry; UC, ulcerative colitis; WT, wild-type; XBP1, X-box binding protein 1.

© 2025 The Author(s). Published by Elsevier Inc. on behalf of the AGA Institute. This is an open access article under the CC BY license (<http://creativecommons.org/licenses/by/4.0/>).

0016-5085

<https://doi.org/10.1053/j.gastro.2025.08.040>

S100A8 and S100A9 exert divergent biological actions. For example, human S100A8 and S100A9 homodimers, but not the S100A8/S100A9 heterotetramer (CP), induced tumor necrosis factor- α production in monocytes.¹³ In mice, *S100a9* gene inactivation decreased experimental autoreactive cluster of differentiation (CD) 8⁺ T cells¹⁴ and modulated psoriasis-like inflammation,^{15,16} supporting the inflammatory nature of S100A9-containing complexes in experimental models beyond the intestine.

Here, we study the protein configurations of S100A8 and S100A9 in human stool from patients with IBD, systematically define their biological actions on human intestinal epithelium and T cells, and delineate inflammatory mechanisms in the gut of mice. We report abundant S100A9 dimers in stool from patients with active IBD, which associates with clinical and endoscopic disease activity, and that homodimers act in an inflammatory manner in the intestine by inducing cytokine responses from human colonic epithelium and by enhancing human CD4⁺ and CD8⁺ T-cell activation.

Materials and Methods

Human Studies

The IBDome cohort comprises patients from a multicenter phenotyping approach of IBD patients from Germany, with patient characteristics summarized in [Supplementary Table 1](#). The phenotypic core and the related transcriptional landscape, as assessed by bulk RNA sequencing in patients with IBD and matched controls, is described as a part of an independent manuscript.¹⁷ Protein studies on fecal CP were performed in IBD patients at the Gastroenterology Outpatient Clinic of the Department of Internal Medicine, Medical University of Innsbruck, who were diagnosed by clinical, endoscopic, and histopathologic means with a disease duration >3 months and who provided informed consent to analyze clinical and biochemical parameters. Age-matched healthy volunteers (n = 34), with no history or biochemical evidence of gastrointestinal disease, served as controls. Investigations were performed in accordance with the Medical University of Innsbruck Ethics Committee (AN4994).

Stool samples from 316 patients from the 1000IBD cohort in Groningen, Netherlands,¹⁸ as well as 84 fecal aspirates from an independent IBD cohort in Kiel, Germany (AZD489/14) were analyzed, with patient characteristics summarized in [Supplementary Tables 2–5](#). Clinical disease activity was determined on the basis of validated disease score indices and biochemical evidence of inflammation. CP configurations in stool were studied by size-exclusion chromatography coupled with liquid chromatography-tandem mass spectrometry (LC-MS/MS) and S100A8 and S100A9 concentration in stool was determined by ELISA as detailed in the [Supplementary Materials and Methods](#). Moreover, we report a protein interaction network of fecal S100A8 and S100A9 in IBD after co-immunoprecipitation and LC-MS/MS.

Mice

All mice were kept in a specific pathogen-free facility at the Medical University of Innsbruck. The following transgenic mouse strains were used on a C57BL/6J background: *S100a9*^{-/-} mice,¹⁵ *Gpx4*^{fllox/wt}; *Villin-Cre*⁺ (*Gpx4*^{+/-IEC}),¹⁹ *Xbp1*^{fllox/fllox}; *Villin-Cre*⁺ (*Xbp1*^{-/-IEC}),²⁰ *Il10*^{-/-} (Jackson Laboratory), and *Rag1*^{-/-}

(Jackson Laboratory). *S100a9*^{-/-} mice were crossed onto *Gpx4*^{+/-IEC} and *Xbp1*^{-/-IEC} mice to obtain double-mutant mice. Genotyping was performed from genomic DNA extracted from ear biopsy specimens of the respective mouse strain. All experiments were conducted in accordance with institutional guidelines and with the approval of the relevant authorities (2021-0.209.767, 2023-0.839.372, 2024-0.019.456, and 2025-0.333.471). Experiments were performed with sex- and age-matched 7- to 9-week-old mice, unless stated otherwise. Treatment groups were assigned randomly, and treatments and dietary regimens are detailed below.

Enteritis and Colitis Models

S100a9^{-/-} mice were orally exposed to 100 μ g of S100A8 or S100A9 or the 1:1 mix of S100A8/S100A9 dissolved in phosphate-buffered saline containing 0.1% bovine serum albumin for 4 consecutive days. A vehicle-treated mouse in the same cage served as a control.

To assess the role of human S100A8 and S100A9 in acute intestinal inflammation, we applied the following approach: First, C57BL/6J wild-type (WT) mice were treated with 2.5% dextran sodium sulfate (DSS; MP Biomedicals, 160110) to induce colitis. DSS was replaced with tap water, and mice were orally exposed to S100A8 (100 μ g/d), S100A9 (100 μ g/d), S100A8/A9 (100 μ g/d) or vehicle once daily for 4 consecutive days until conclusion of the experiment.

Next, DSS colitis was induced in *S100a9*^{-/-} mice using 2% DSS. To analyze the inflammatory potential of S100A8, S100A9, and S100A8/A9 during chronic colitis, *Il10*^{-/-} mice were orally gavaged with 100 μ g of recombinant protein daily for 7 consecutive days. Colitis severity was determined by clinical and histologic means, as previously reported.²¹

Pharmacologic inhibition of S100A9 was performed with oral gavage administration of 10 mg/kg paquinimod (MedChemExpress, HY-100442) once daily for 7 days in WT mice exposed to 2.5% DSS or for 14 days in *Il10*^{-/-} mice (in drinking water). In *Rag1*^{-/-} mice, DSS colitis was induced and 100 μ g of human recombinant S100A8 or S100A9 was orally administered and compared with vehicle, as described above.

Moreover, the impact of human S100A8 and S100A9 on enteritis was determined: *Gpx4*^{+/-IEC} and *Xbp1*^{-/-IEC} mice (and littermate WT controls) were exposed to a polyunsaturated fatty acid-enriched Western diet for 3 months (ssniff, TD88137 plus 10% fish oil) to induce CD-like enteritis in mice,²² with or without exposure to 100 μ g of the human recombinant S100A8, S100A9, or S100A8/S100A9 (1:1 mix) for 7 consecutive days before conclusion of the experiment, whereas vehicle served as a control.

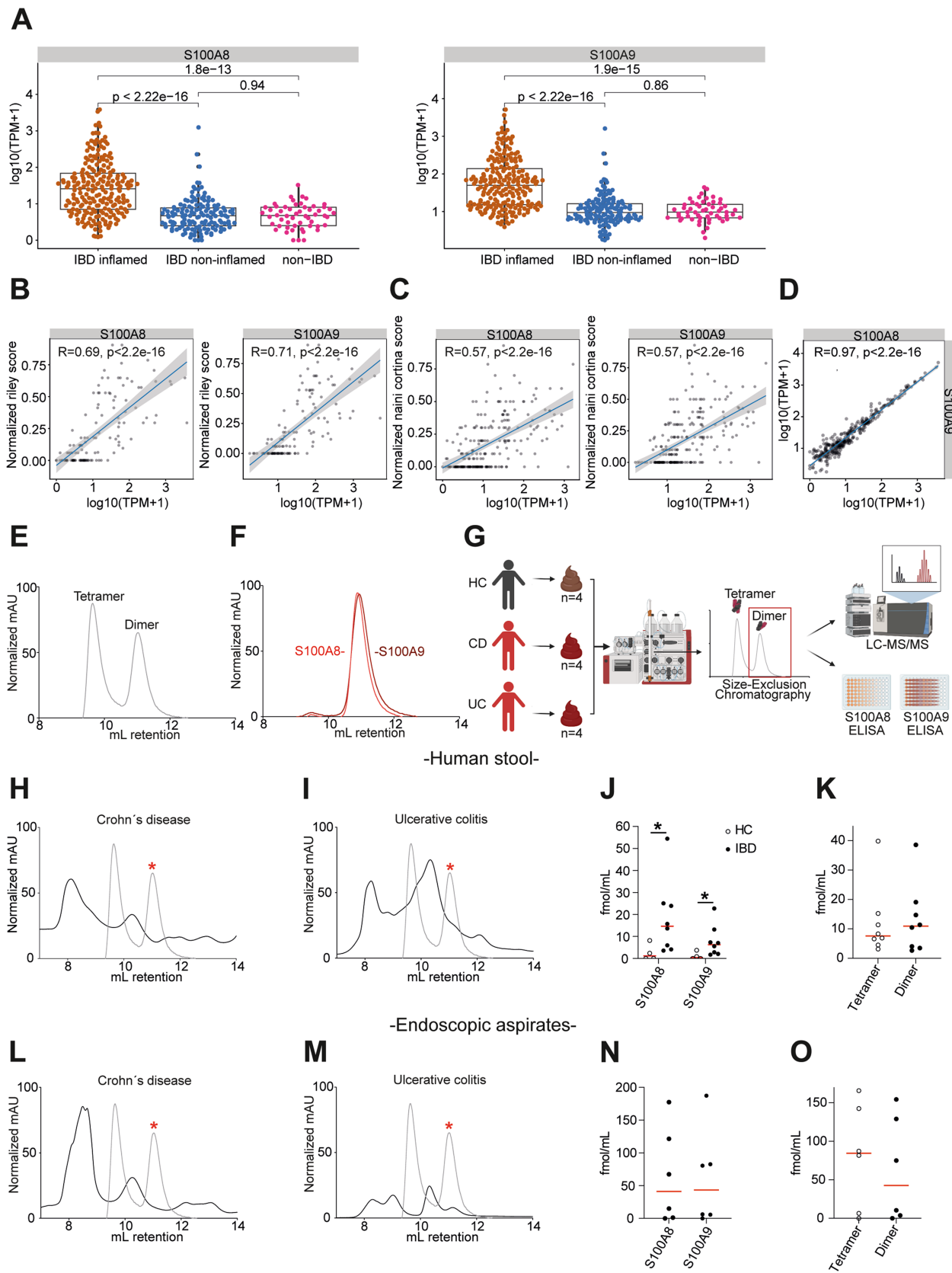
Next, *S100a9*^{-/-}/*Gpx4*^{+/-IEC} double-mutant mice and respective controls were exposed to a polyunsaturated fatty acid-enriched Western diet for 3 months, *S100a9*^{-/-}/*Xbp1*^{-/-IEC} double-mutant mice and respective controls were exposed to a chow diet, and enteritis was evaluated by clinical and histologic means. Molecular assays used to study enteritis and colitis phenotypes are detailed in the [Supplementary Materials and Methods](#).

Experimental Approach With Human Colonic Epithelium and Blood-Derived T Cells

Human differentiated colonic intestinal epithelial organoid monolayers were generated from non-IBD controls and

stimulated with S100A8, S100A9, S100A8/S100A9, or vehicle, and transcriptional profiles of specialized epithelium were analyzed by single-cell RNA sequencing (10X Genomics), as

detailed in the [Supplementary Materials and Methods](#). Human T cells were purified, cultured, and stimulated from peripheral blood mononuclear cells and phenotyped by flow cytometry



and antigen-reactive T-cell enrichment, as detailed in the [Supplementary Materials and Methods](#).

Bioinformatics and Statistical Analysis

RNA sequencing approaches and statistics of human cohorts, and specifically the IBDome cohort, were analyzed as described in the [Supplementary Materials and Methods](#).

Results

Fecal Calprotectin Configurations in Inflammatory Bowel Disease

First, we assessed the transcriptional patterns of *S100A8* and *S100A9* in the human intestine by bulk RNA sequencing of tissue from the small and large intestine of 360 IBD samples (from 246 patients) compared with 54 non-IBD controls from the IBDome cohort (see Materials and Methods), with patient characteristics shown in [Supplementary Table 1](#). *S100A8* and *S100A9* were increasingly expressed in the inflamed intestine in patients with histologic disease activity compared with noninflamed tissue from controls or IBD patients without histologic disease activity ([Figure 1A](#) and [Supplementary Figure 1A](#)). Moreover, mucosal expression of *S100A8* and *S100A9* in patients with CD and UC correlated with endoscopic (and to a lesser extent with clinical) disease activity ([Supplementary Figure 1B–E](#)) and with histologic disease activity ([Figure 1B](#) and [C](#)). Mucosal *S100A8* expression directly correlated with *S100A9* expression in patients with IBD ([Figure 1D](#)), indicating that both proteins are concomitantly expressed in the inflamed intestine, which we corroborated by immunohistochemistry ([Supplementary Figure 1F](#)).

Untargeted proteomics using liquid chromatography (LC) coupled with MS/MS (LC-MS/MS) revealed that CP is abundant in stool from patients with active UC and active CD ([Supplementary Figure 1G](#)), which enabled us to investigate protein configurations of fecal *S100A8* and *S100A9*.

We generated human recombinant *S100A8*, *S100A9*, or the 1:1 mix (CP) ([Supplementary Figure 1H](#)), confirmed the purity ([Supplementary Figure 1I–M](#)), and then used these proteins as a reference for size-exclusion chromatography. We confirmed that the 1:1 mix of human recombinant *S100A8* with *S100A9* formed protein complexes at a size compatible with the calprotectin heterotetramer (CP), and to a lesser extent homo- and heterodimers, which cannot be resolved with this technique ([Figure 1E](#)). Human recombinant *S100A8* spontaneously formed protein complexes at a size compatible with *S100A8*/*S100A8* homodimers, as similarly observed for human recombinant *S100A9* homodimers ([Figure 1F](#) and [Supplementary Figure 1L](#) and [M](#)).

Next, we established size-exclusion chromatography with human stool from 4 non-IBD controls and human recombinant CP as a reference ([Supplementary Figure 1N](#)) and then performed size-exclusion chromatography with stool from 8 patients with active IBD (4 active UC and 4 active CD with fecal calprotectin >500 $\mu\text{g/g}$). We analyzed whether a fraction retrieved from size-exclusion chromatography at molecular sizes compatible with homo-heterodimers (as largely determined by the hydrodynamic radius) enabled detection of *S100A8* or *S100A9* by LC-MS/MS and by ELISA ([Figure 1G](#)).

Most notably, size-exclusion chromatography fractions from active CD and UC patients contained *S100A8* and *S100A9* at sizes compatible with homo-/heterodimers ([Figure 1H](#) and [I](#)), as indicated by LC-MS/MS ([Figure 1J](#)) and by ELISA ([Supplementary Figure 1O](#)). Notably, the

Figure 1. Detection of *S100A8* and *S100A9* dimers in stool from patients with IBD. (A) Box plots illustrating the mucosal expression levels of *S100A8* and *S100A9* in patients with inflamed and noninflamed IBD and non-IBD controls from the IBDome cohort, with *P* values retrieved with the Wilcoxon-Mann-Whitney test. The boxes indicate the 25th percentile (bottom border), median (center line), and 75th percentile (top border), and the whiskers extend to data points within 1.5* IQR (interquartile range) of the lower and upper quartiles. TPM, transcripts per million. Correlation between mucosal expression of *S100A8* and *S100A9* with histologic disease activity (B) in patients with UC assessed by the normalized Riley score, and (C) in patients with CD assessed by the normalized Naini Cortina score. (D) Correlation of mucosal *S100A8* and *S100A9* expression in the IBDome cohort. (E) Representative size-exclusion chromatography (SEC) spectra of human recombinant *S100A8*/*S100A9* (CP), (F) and the overlay of human recombinant *S100A8* homodimers and *S100A9* homodimers. mAU, milli absorbance unit. (G) Schematic overview of the approach. SEC of human stool was coupled with LC-MS/MS and *S100A8* and *S100A9* ELISAs. The chromatography spectrum of human stool was compared with that of human recombinant protein, and fractions at a size compatible with dimers were analyzed with LC-MS/MS and *S100A8*- and *S100A9*-specific ELISA. HC, healthy control. Image was created in <https://BioRender.com>. (H) Representative SEC spectra of stool specimen dissolved in phosphate-buffered saline from patients with CD (*n* = 4) and (I) from patients with UC (*n* = 4). Gray spectra indicate chromatographic peaks of human recombinant *S100A8* and *S100A9* dimers indicated by a red asterisk. SEC fractions at this size were retrieved for detection of *S100A8* and *S100A9* by LC-MS/MS. (J) Quantification of *S100A8* and *S100A9* concentration in SEC fractions (of stool) compatible with homo-/heterodimers by LC-MS/MS with spike-in experiments (see Materials and Methods) (*n* = 4/8). (K) Quantification of *S100A8* and *S100A9* concentration in SEC fractions (of stool) by LC-MS/MS with spike-in experiments (*n* = 8/8). Depicted is the average of *S100A8* and *S100A9* concentration per patient from the SEC fraction that corresponds to the dimer fraction compared with the tetramer fraction. Representative SEC spectra of endoscopy washes from (L) CD patients (*n* = 3) and (M) UC patients (*n* = 3). (N) Quantification of *S100A8* and *S100A9* concentration in SEC fractions (of endoscopy washes) compatible with homo-/heterodimers by LC-MS/MS with spike-in experiments (*n* = 6/6). (O) Quantification of *S100A8* and *S100A9* concentration in SEC fractions (of endoscopy washes) by LC-MS/MS with spike-in experiments (*n* = 6/6). Depicted is the average of *S100A8* and *S100A9* concentration from the SEC fraction that corresponds to the dimer fraction, when compared with the tetramer fraction. **P* < .05.

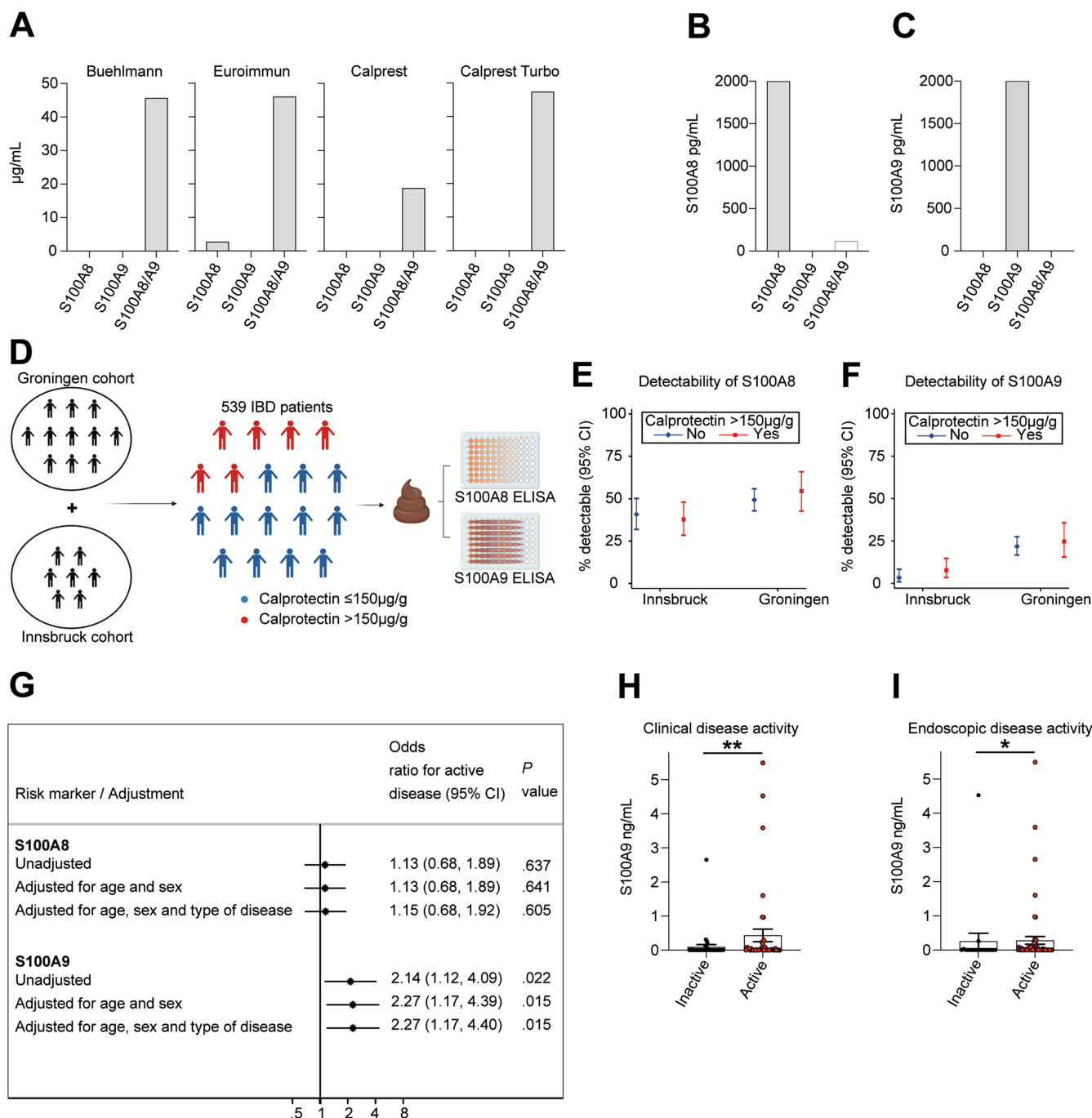


Figure 2. Quantification of S100A8 and S100A9 in relation to IBD activity. (A) Quantification of human recombinant S100A8, S100A9, and S100A8/S100A9 (CP) with indicated ELISAs used in clinical routine. Quantification of human recombinant (B) S100A8 and (C) S100A9 with commercial research ELISAs. (D) Schematic overview of the approach. We analyzed stool from 539 patients of 2 IBD cohorts from Innsbruck (Austria, $n = 223$) and Groningen (the Netherlands, $n = 316$). The concentration of fecal CP exceeded $150 \mu\text{g/g}$ stool in 180 patients, and the remaining patients were characterized by CP levels $\leq 150 \mu\text{g/g}$. All stool samples were then analyzed by specific S100A8 and S100A9 ELISA. Image was created in <https://BioRender.com>. Percentage of IBD patients with fecal CP levels $\leq 150 \mu\text{g/g}$ or $>150 \mu\text{g/g}$ from the Innsbruck and Groningen cohorts with detectable (E) S100A8 or (F) S100A9 protein in stool, as determined by ELISA (95% confidence interval [CI]). (G) Association of fecal detection of S100A8 or S100A9 in patients with clinical disease activity and fecal CP concentration $\leq 150 \mu\text{g/g}$, as determined by logistic regression modeling, with and without adjustment for age, sex, and type of disease. CI, confidence interval. Quantification of S100A9 concentration in endoscopic aspirates from the colon of IBD patients with CP concentration $\leq 150 \mu\text{g/mL}$ in IBD patients stratified by (H) clinical disease activity or (I) endoscopic disease activity in a cohort from Kiel, Germany ($n = 84$) (mean \pm SEM shown; Mann-Whitney U test). * $P < .05$, ** $P < .01$.

concentration of S100A8 and S100A9 homo-/heterodimers was comparable to that of the heterotetramer (CP) in the respective size-exclusion chromatography fractions (Figure 1K). By contrast, stool from non-IBD controls did not show evidence of S100A8 and S100A9 homo-/heterodimers in the specific size-exclusion chromatography fractions (Figure 1J and Supplementary Figure 1O).

Moreover, analysis of endoscopy-retrieved fecal colonic aspirates from patients with active IBD (3 CD and 3 UC patients) validated the presence of S100A8 and S100A9 homo-/heterodimers, as indicated by LC-MS/MS and by ELISA (Figure 1L–N and Supplementary Figure 1P). The concentration of S100A8 and S100A9 homo-/heterodimers were similar to those of the heterotetramer (CP) in the respective size-exclusion chromatography fractions (Figure 1O). Collectively, these studies demonstrated that the mucosal expression of *S100A8* and *S100A9* correlated with clinical, endoscopic, and histologic disease activity and that S100A8 and S100A9 homo-/heterodimers were detectable in patients with active IBD in addition to the heterotetramer (CP).

S100A8 and S100A9 Dimer Detection in Inflammatory Bowel Disease

These findings led us to assess the diagnostic utility of S100A8 and S100A9 dimer detection in IBD. Four fecal CP assays used in clinical routine neither detected human recombinant S100A8 nor S100A9 homodimers (Figure 2A), while detecting the 1:1 mix of the human recombinant S100A8/S100A9 heterotetramer (CP), indicating a diagnostic gap of current clinical assays in the detection of S100A8 and S100A9 dimers. Consequently, we used specific ELISAs (established for research use) that allowed detection of human recombinant S100A8 and S100A9 homodimers, without detecting the S100A8/S100A9 heterotetramer (CP) (Figure 2B and C), to estimate their presence and concentration in stool from patients with IBD. We analyzed the stool from 539 patients of 2 IBD cohorts from Innsbruck (Austria, $n = 223$) and Groningen (the Netherlands, $n = 316$) (Figure 2D), with patient characteristics listed in Supplementary Table 2. More specifically, 338 patients (63%) were diagnosed with CD and 201 patients (37%) with UC. CP was detectable ($>16 \mu\text{g/g}$) in 413 patients (77%), and the concentration was $>150 \mu\text{g/g}$ stool in 180 patients (33%). Across all patients, fecal S100A8 was detectable in 248 patients (46%), with a median concentration of 5.0 ng/g , and fecal S100A9 was detectable in 83 patients (15%), with a median concentration of 5.4 ng/g , which was unrelated to fecal CP concentration (Figure 2E and F). In line, we did not note a correlation between fecal CP and S100A8 or S100A9 concentration (Supplementary Figure 2A and B). Thirty-four adults without a history of IBD and without gastrointestinal symptoms (non-IBD controls) did not exhibit detectable levels of S100A9 in stool, while 7 of 34 healthy controls exhibited minute evidence for S100A8 (Supplementary Figure 2C). These findings indicated that fecal S100A8 and S100A9 dimer detection

was frequently demonstrable in patients with IBD independent from fecal CP concentration.

Fecal CP is used in clinical practice as a biomarker to help identify patients with active disease, with $>150 \mu\text{g/g}$ CP in stool suggesting an inflammatory condition in patients with IBD.²³ However, symptoms compatible with active IBD are commonly reported in patients with fecal CP $<150 \mu\text{g/g}$, indicating a limitation of fecal CP as a biomarker that comes along with uncertainty in clinical management.

Therefore, we next assessed the utility of S100A8 and S100A9 detection in patients with symptomatic disease (ie, clinical disease activity) and fecal CP $\leq 150 \mu\text{g/g}$ in the cohort from Innsbruck and Groningen. Among the 356 patients with available disease activity scores and a fecal CP concentration $\leq 150 \mu\text{g/g}$ stool, 75 (21%) had clinically active disease and 281 (79%) were in remission (Supplementary Table 2).

By logistic regression modeling (without adjustment for age, sex, type of disease), we noted that fecal detection of S100A9, but not detection of S100A8, was associated with 2.14-fold odds of having clinically active disease (95% confidence interval, 1.12–4.09; $P = .022$). The association between S100A9 and clinically active disease remained robust when adjusting for age and sex (odds ratio, 2.27; 95% confidence interval, 1.17–4.39, $P = .015$), and additionally for disease type (odds ratio, 2.27; 95% confidence interval, 1.17–4.40; $P = .015$) (Figure 2G). Neither disease location (Montreal L1–L3) nor smoking status (current smoker) associated with detection of fecal S100A8 or S100A9 dimers (Supplementary Tables 3 and 4).

We corroborated these results by comparison of endoscopy reports and clinical disease assessment with ELISA-based colonic aspirate quantification of S100A9 in 84 patients with IBD from Kiel, Germany (Supplementary Table 5). Indeed, detection of S100A9 was associated with clinical disease activity (Figure 2H) and with endoscopic disease activity (Figure 2I) in patients with low CP concentration ($\leq 150 \mu\text{g/mL}$). Notably, detection of S100A8 in colonic aspirates was also associated with endoscopic but not clinical disease activity (Supplementary Figure 2D and E).

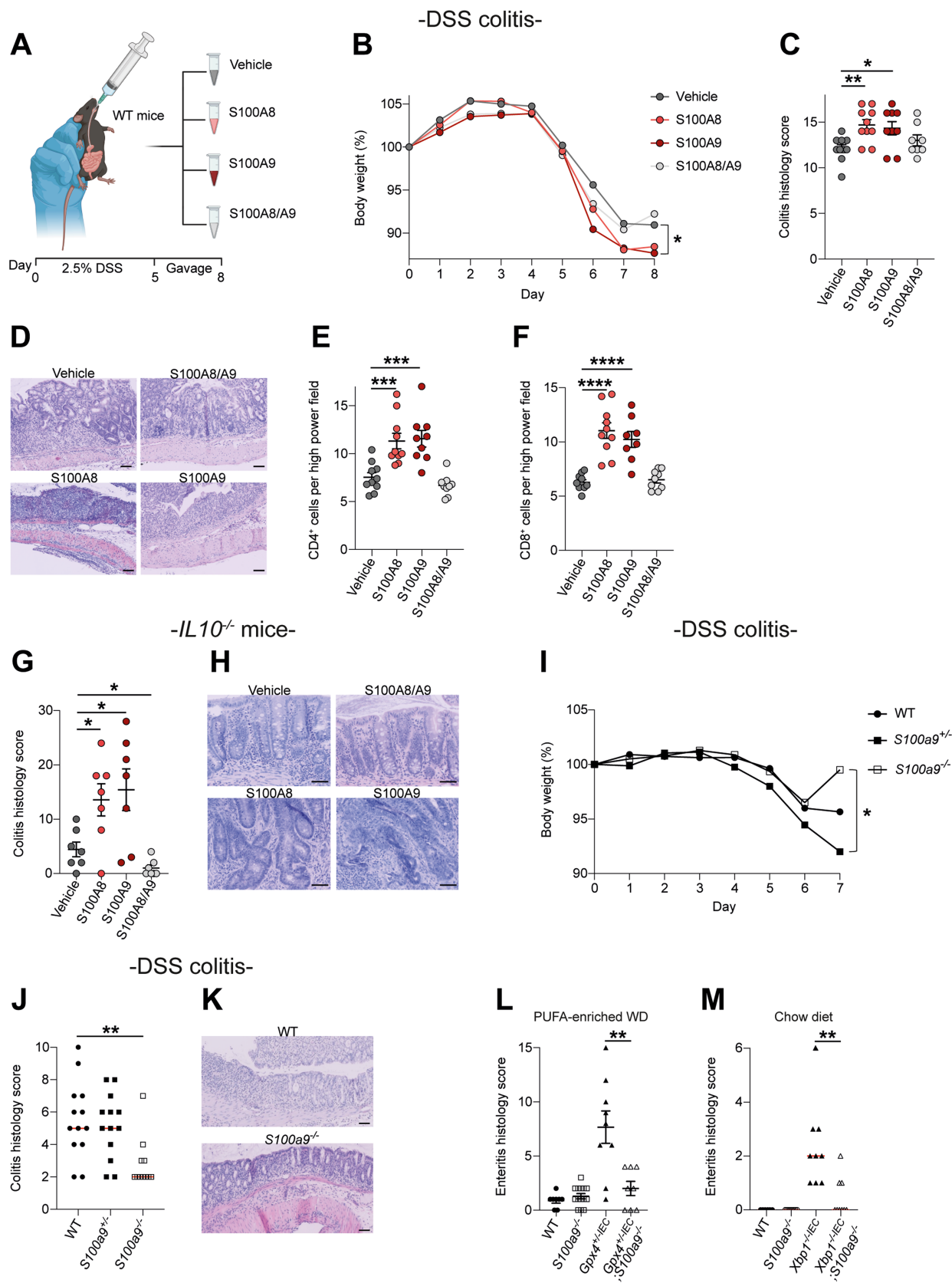
Collectively, these studies demonstrated that S100A8 and S100A9 were commonly detectable in the human intestine and stool of patients with IBD and that fecal S100A9 concentration was associated with clinical and endoscopic disease activity in patients with low fecal CP concentration ($\leq 150 \mu\text{g/g}$). Larger endoscopy trials are warranted to determine the utility of S100A8 and S100A9 as biomarkers for active IBD in clinical practice.

Human S100A8 and S100A9 Homodimers Promote Enteritis and Colitis in Mice

Because we identified luminal S100A8 and S100A9 dimers in stool and colonic aspirates from patients with IBD, we rationalized that oral gavage of human S100A8 and S100A9 dimers should enable the study of their biological

effect in the mouse intestine. Indeed, oral gavage of human recombinant S100A8 and S100A9 homodimers led to distribution along the murine gastrointestinal tract and was

specifically detectable in small intestinal mucosa, gut epithelium, and colonic content ([Supplementary Figure 3A and B](#)). Likewise, S100A8 and S100A9 homodimers were



taken up by MODE-K intestinal model epithelium (Supplementary Figure 3C and D). We exposed WT mice to 2.5% DSS and orally gavaged S100A8 homodimers, S100A9 homodimers, the S100A8/S100A9 heterotetramer (CP), or vehicle for 4 consecutive days starting at day 5 when colitis was established (Figure 3A). S100A8 and S100A9 homodimers, but not the heterotetramer (CP), promoted DSS colitis compared with vehicle, indicated by clinical and histologic means (Figure 3B–D). S100A8 and S100A9 homodimers also promoted DSS colitis in *S100a9*^{−/−} mice (Supplementary Figure 3E and F), which lack S100A9-containing species and expressed no S100A8 in the gut (Supplementary Figure 3G and H), suggesting that the inflammatory effect of S100A8 and S100A9 homodimers could not be explained by chimeric effects of human with mouse protein in this model. Notably, S100A8 and S100A9 homodimers increased CD4⁺ and CD8⁺ T-cell infiltration in the inflamed mucosa (Figure 3E and F and Supplementary Figure 3I and J).

In line, oral gavage of S100A8 and S100A9 homodimers for 7 consecutive days, but not CP, promoted chronic colitis in *Il10*^{−/−} mice (Figure 3G and H). Moreover, S100A8 or S100A9 homodimers, but not CP, worsened experimental enteritis in *Gpx4*^{+/−IEC} and in *Xbp1*^{−/−IEC} mice (Supplementary Figure 3K and L), which was induced by a model Western diet for 3 months.^{19,22} Conversely, genetic inactivation of *S100a9* protected against experimental gut inflammation. *S100a9*^{−/−} mice were protected against DSS colitis compared with heterozygous *S100a9*^{+/−} or WT mice (Figure 3I–K). Inactivation of *S100a9* also ameliorated experimental enteritis in *Gpx4*^{+/−IEC} mice (induced by a model Western diet), and spontaneous enteritis in *Xbp1*^{−/−IEC} mice (Figure 3L and M and Supplementary Figure 3M and N). Collectively, these data demonstrated that human S100A8 and S100A9 homodimers worsened experimental enteritis and colitis in mice and, vice versa, that genetic inactivation of *S100a9* ameliorated experimental enteritis and colitis.

Human S100A8 and S100A9 Homodimers Induce an Inflammatory Response in Intestinal Epithelium

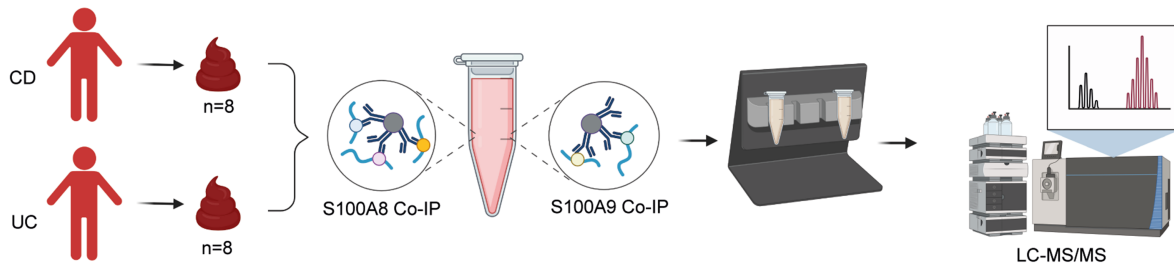
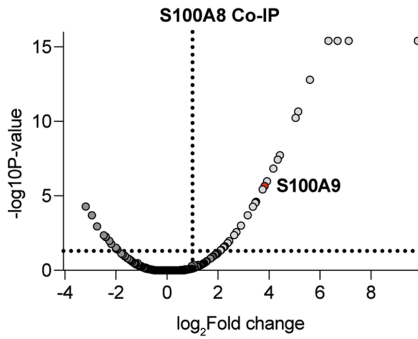
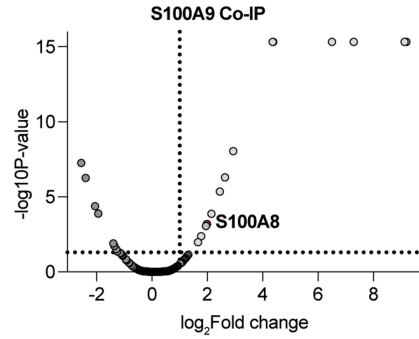
Next, we investigated inflammatory effects of human S100A8 and S100A9 homodimers. In a first step, we

performed antibody-mediated immunoprecipitation of S100A8 and S100A9 dimers from stool of 16 patients with active IBD and consequently defined the fecal protein interaction network by means of untargeted LC-MS/MS (Figure 4A). S100A8 interacted with S100A9 (and vice versa) in stool from patients with active IBD (Figure 4B and C), demonstrating the validity of our approach. Several protein interaction partners of S100A8 and S100A9 in stool from active IBD patients were identified with this approach (Supplementary Tables 6 and 7), some of them suggesting actions at the intestinal epithelium (eg, interaction with galectin-4 and matrix metalloproteinase 15). Thus, we used single-cell RNA sequencing of differentiated human colonic organoids upon stimulation with S100A8 or S100A9 homodimers to determine the transcriptional response of specialized intestinal epithelium when compared with vehicle exposure (Figure 4D). Indeed, S100A8 and S100A9 homodimers broadly induced cytokine expression in differentiated colonocytes, for example, chemokine ligand 20 in goblet cells (Figure 4E). Moreover, Pathway RespOnsive GENes for activity inference (PROGENy) pathway activity analysis indicated that S100A8 homodimers induced a transcriptional tumor necrosis factor and nuclear factor- κ B response in colonocytes, compared with vehicle, and that S100A9 induced hypoxia signaling (Figure 4F). Collectively, these data indicated that S100A8 and S100A9 homodimers induce an inflammatory response in human intestinal epithelium.

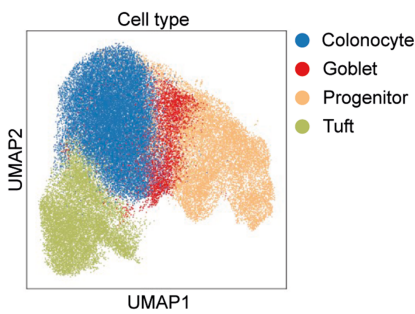
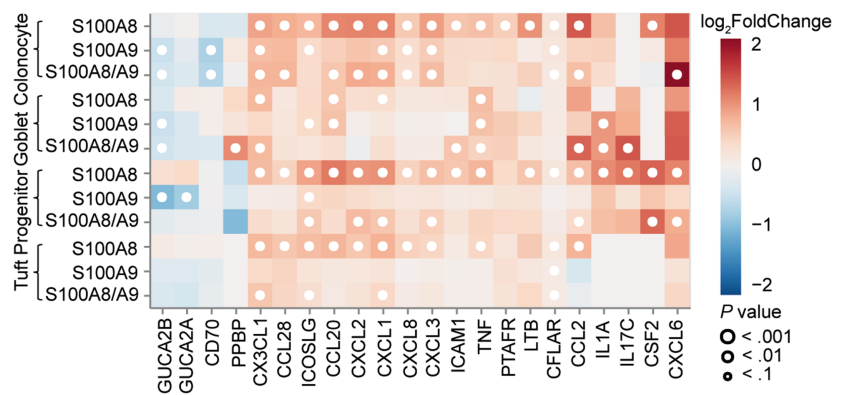
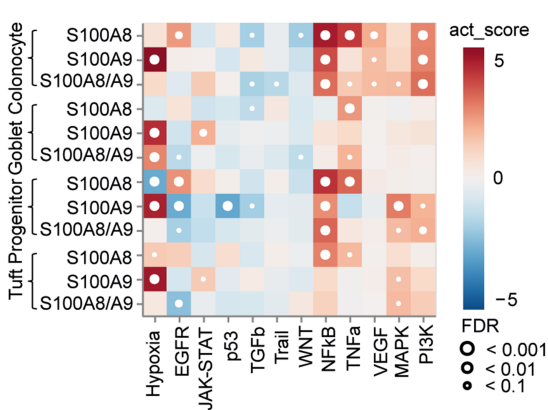
Human S100A8 and S100A9 Homodimers Enhance Cluster of Differentiation 4-Positive and 8-Positive T-Cell Activation

Oral exposure to human S100A9 homodimers promoted the recruitment of CD8⁺ T cells into the mucosa of *S100a9*^{−/−} mice (Supplementary Figure 4A–L), without histologic signs of gut inflammation (Supplementary Figure 5A and B). For this reason, we explored the impact of S100A8 and S100A9 homodimers on CD4⁺ and CD8⁺ T cells that are critically involved in chronic gut inflammation in IBD.²⁴ We purified CD4⁺ and CD8⁺ T cells from the blood of 6 healthy donors and exposed these cells to S100A8 or S100A9 homodimers, CP, or vehicle, followed by immunophenotyping by flow cytometry (Figure 5A). S100A8 and

Figure 3. Human S100A8 and S100A9 homodimers promote enteritis and colitis in mice. (A) Schematic representation of approach: WT mice were exposed to 2.5% DSS for 5 days and subsequently exposed to 100 μ g S100A8 or S100A9, the S100A8/S100A9 1:1 mix (CP), or vehicle by gavage once daily for 4 days. Image was created in <https://BioRender.com>. (B) Body weight course of mice, with (C) colitis histology score at day 8 (n = 8–10; 8–9 weeks; mean \pm standard error of the mean [SEM] shown; 1-way analysis of variance [ANOVA] with post hoc Bonferroni) and (D) representative H&E images. Scale bars, 100 μ m. Quantification of (E) CD4⁺ T cells and (F) CD8⁺ T cells in the colon of WT mice (scored in Figure 1C), as determined by immunohistochemistry (mean \pm SEM shown; 1-way ANOVA with post hoc Bonferroni). (G) Colitis histology score and (H) representative H&E images of *Il10*^{−/−} mice after oral exposure to vehicle, S100A8, S100A9 or the 1:1 mix (CP) (n = 7 each; 8–9 weeks; 1-way ANOVA with post hoc Holm's correction; mean \pm SEM). Scale bars, 100 μ m. (I) Body weight course of mice, with (J) colitis histology score and (K) representative H&E images of WT (n = 13), *S100a9*^{+/−} (n = 13), and *S100a9*^{−/−} (n = 11) mice after 5 days of DSS (8–9 weeks; Kruskal-Wallis test with Dunn's correction; median shown). Scale bars, 100 μ m. (L) Enteritis histology score of *Gpx4*^{+/−IEC} (n = 9) and *Gpx4*^{+/−IEC}; *S100a9*^{−/−} (n = 8) mice fed a polyunsaturated fatty acid (PUFA)-enriched Western diet (WD) for 3 months (mean \pm SEM shown, 2-tailed Student *t* test). (M) Enteritis histology score of *Xbp1*^{−/−IEC} (n = 9) and *Xbp1*^{−/−IEC}; *S100a9*^{−/−} (n = 9) mice fed a chow diet (7–8 weeks; median shown, Mann-Whitney *U* test). **P* < .05, ***P* < .01, ****P* < .001, *****P* < .0001.

A**B****C**

-Single-cell RNA Sequencing-

D**E****F**

S100A9 homodimers promoted the activation of CD4⁺ and CD8⁺ effector T cells and effector memory CD45RO⁺ T cells, by enhancing CD25 and CD69 up-regulation upon T-cell receptor stimulation compared with vehicle (Figure 5B–G and Supplementary Figure 6B–J). Moreover, S100A9 homodimers increased granzyme B-expressing CD8⁺ T cells (Figure 5H), and S100A8 and S100A9 homodimers induced the production of interleukin 17A, but not interferon gamma or tumor necrosis factor, in CD3⁺ T cells (Figure 5I and Supplementary Figure 6J and K). Furthermore, S100A8 and S100A9 homodimers induced a transcriptional nuclear factor- κ B and Janus kinase/signal transducer and activator of transcription signature compared with vehicle, as assessed by bulk RNA sequencing of CD8⁺ T cells (Figure 5J), which we confirmed by immunoblotting (Figure 5K and L and Supplementary Figure 6L–N).

We further analyzed antigen-specific CD4⁺ T-cell activation by S100A8 and S100A9 using antigen-reactive CD4⁺ T-cell enrichment.^{25,26} We detected reactive memory CD4⁺ T cells against S100A9 homodimers, as compared to vehicle (Supplementary Figure 6O). Collectively, these studies demonstrated that human S100A8 and S100A9 homodimers enhance the activation of CD4⁺ and CD8⁺ T cells.

Inflammatory Actions of S100A8 and S100A9 Homodimers Require Adaptive Immunity in Mice

Finally, we validated that human S100A8 and S100A9 homodimers promote intestinal inflammation by induction of adaptive immunity. We induced colitis by DSS in *Rag1*^{−/−} mice that lack adaptive immunity and orally exposed mice to human S100A8 or S100A9 homodimers or vehicle for 4 consecutive days. The inflammatory effect of S100A8 and S100A9 homodimers was comparable to that of vehicle in *Rag1*^{−/−} mice during DSS colitis (Figure 6A–C). These findings demonstrate that proinflammatory actions of S100A8 and S100A9 homodimers were dependent on adaptive immunity, which orchestrate chronic gut inflammation.²⁷ Moreover, pharmacologic inhibition of S100A9 with paquinimod (Supplementary Figure 7A) protected WT mice against DSS colitis (Figure 6D and E), and *Il10*^{−/−} mice

against chronic colitis (Figure 6F and G). Collectively, our approach demonstrates that human S100A8 and S100A9 homodimers promote experimental colitis by inducing adaptive immune responses and that chronic colitis can be ameliorated by pharmacologic inhibition of S100A9.

Discussion

IBDs comprise a spectrum of chronic inflammatory disorders with heterogeneous clinical manifestations and a variable response to medical therapy.^{3,4} Despite this complexity, most patients with active IBD exhibit CP in stool, with a fecal CP concentration >150 μ g/g being compatible with active disease in symptomatic patients.^{5,6} Understanding the configuration and related biological actions of S100A8 and S100A9 in the human intestine harbors the potential for biomarker discovery in inflammatory conditions of the intestine and may enable therapeutic targeting of a molecular driver of intestinal inflammation in IBD.

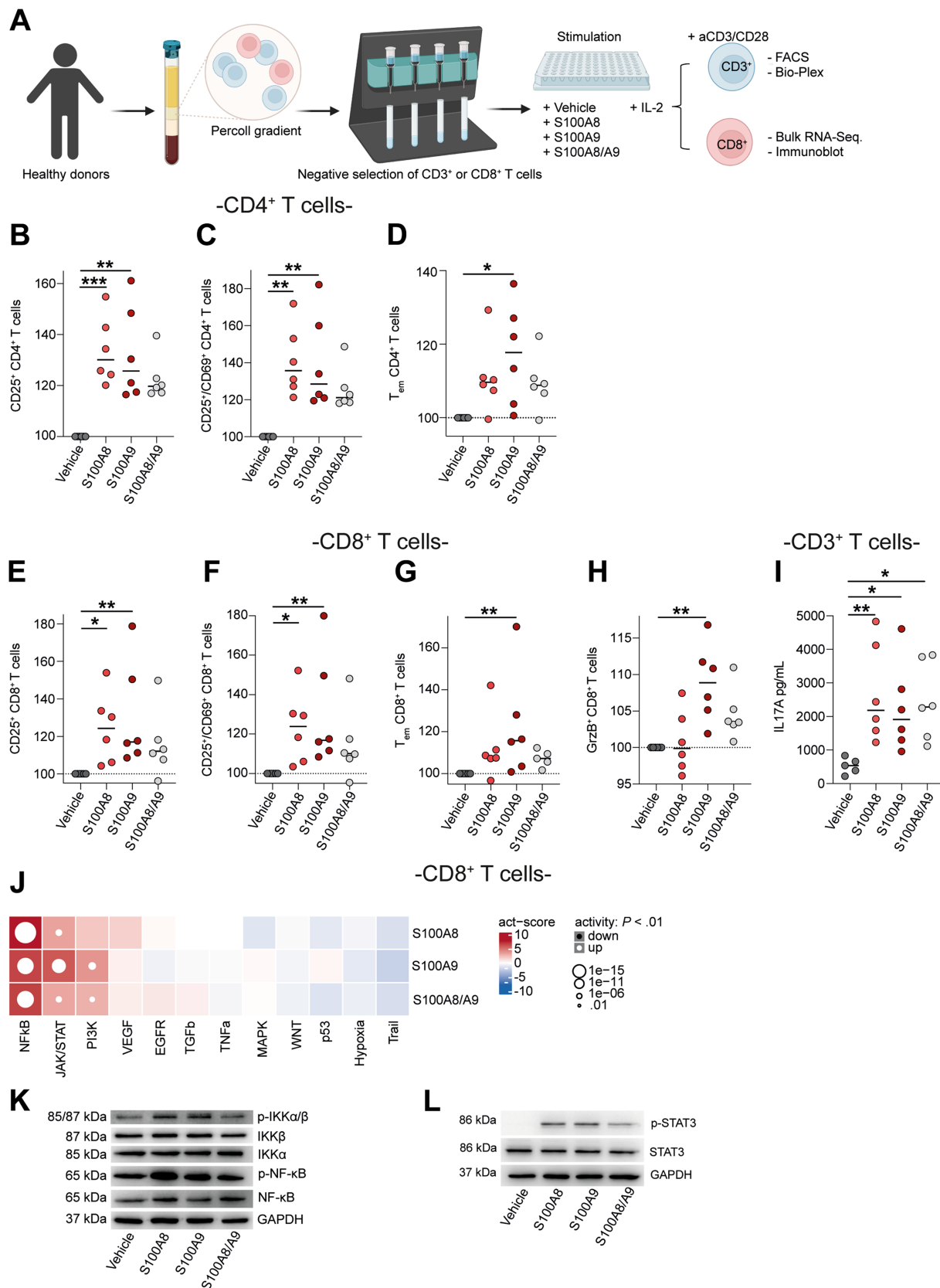
Here, we reveal the presence of abundant S100A8 and S100A9 homo-/heterodimers in addition to CP in stool from adults with IBD by size-exclusion chromatography coupled with LC-MS/MS. Tissue transcriptomics from the IBDome cohort¹⁷ indicated that *S100A8* and *S100A9* were concomitantly expressed in the inflamed mucosa of patients with IBD and that their expression correlated with clinical, endoscopic, and histologic disease activity. By fecal analysis of IBD patients from 2 independent cohorts in Groningen and Innsbruck, we report that S100A8 dimers were detected in 48% and S100A9 dimers were detected in 15% of IBD patients. Fecal S100A9 detection, but not S100A8 detection, provided odds for clinical disease activity in patients with low fecal CP concentration (≤ 150 μ g/g). In an independent cohort from Kiel, Germany, we demonstrate that luminal S100A9 detection associated with clinical and endoscopic disease activity in colonic aspirates from patients with IBD.

Our preclinical studies demonstrate that oral exposure to human S100A8 and S100A9 homodimers, but not CP, worsened gut inflammation in 4 independent mouse models to a comparable extent. In turn, genetic inactivation

Figure 4. Human S100A8 and S100A9 homodimers induce epithelial cytokine responses. (A) Schematic representation of co-immunoprecipitation (Co-IP) experiments performed for identification of protein interaction partners of S100A8 and S100A9 in the gut lumen of IBD patients shown in B and C. Image was created in <https://BioRender.com>. Volcano plot depicting protein interaction partners of (B) S100A8 and (C) S100A9 in stool from patients with active IBD (CD, n = 8; UC, n = 8), as identified by LC-MS/MS analysis after Co-IP. Significant protein interactions are defined by a *P* value <.05 and a fold change of >2. (D) Single-cell RNA sequencing of human colonic organoids, differentiated into monolayers, with Uniform Manifold Approximation and Projection (UMAP) projection depicting epithelial cell populations. (E) Heat map showing differential cytokine gene expression per cell-type in differentiated organoids treated with S100A8, S100A9, or S100A8/S100A9 (1:1), relative to vehicle. Red indicates up-regulation of cytokine expression, blue indicates down-regulation. (F) Pathway RespOnsive GENes for activity inference (PROGENy) pathway activity scores (using a multivariate linear model) per epithelial cell type in differentiated organoids exposed to S100A8, S100A9, or S100A8/S100A9 (1:1). Red indicates up-regulation of a pathway relative to vehicle. CCL, chemokine (C-C motif) ligand; CFLAR, CASP8 and FADD like apoptosis regulator; CSF2, colony-stimulating factor 2; CX3CL1, C-X3-C motif chemokine ligand 1; CXCL, chemokine (C-X-C motif) ligand; EGFR, epidermal growth factor receptor; FDR, false discovery rate; GUCY, guanylate cyclase activator; ICAM, intercellular adhesion molecule; ICOSL, inducible co-stimulator ligand; IL, interleukin; LTB, lymphotoxin-beta; MAPK, mitogen-activated protein kinase; NF- κ B, nuclear factor- κ B; PI3K, phosphatidylinositol-3-kinase; PPBP, pro-platelet basic protein; PTAFR, platelet-activating factor receptor; JAK/STAT, Janus kinase/signal transducer and activator of transcription; TGF, transforming growth factor; TNF, tumor necrosis factor; TRAIL, TNF-related apoptosis-inducing ligand; VEGF, vascular endothelial growth factor.

of *S100a9* protected against experimental gut inflammation in mice. Transcriptional phenotyping of human colonic epithelium and T cells, coupled with mechanistic studies in

transgenic mice, portray a mechanism by which S100A8 and S100A9 homodimers promote chronicity of inflammation.



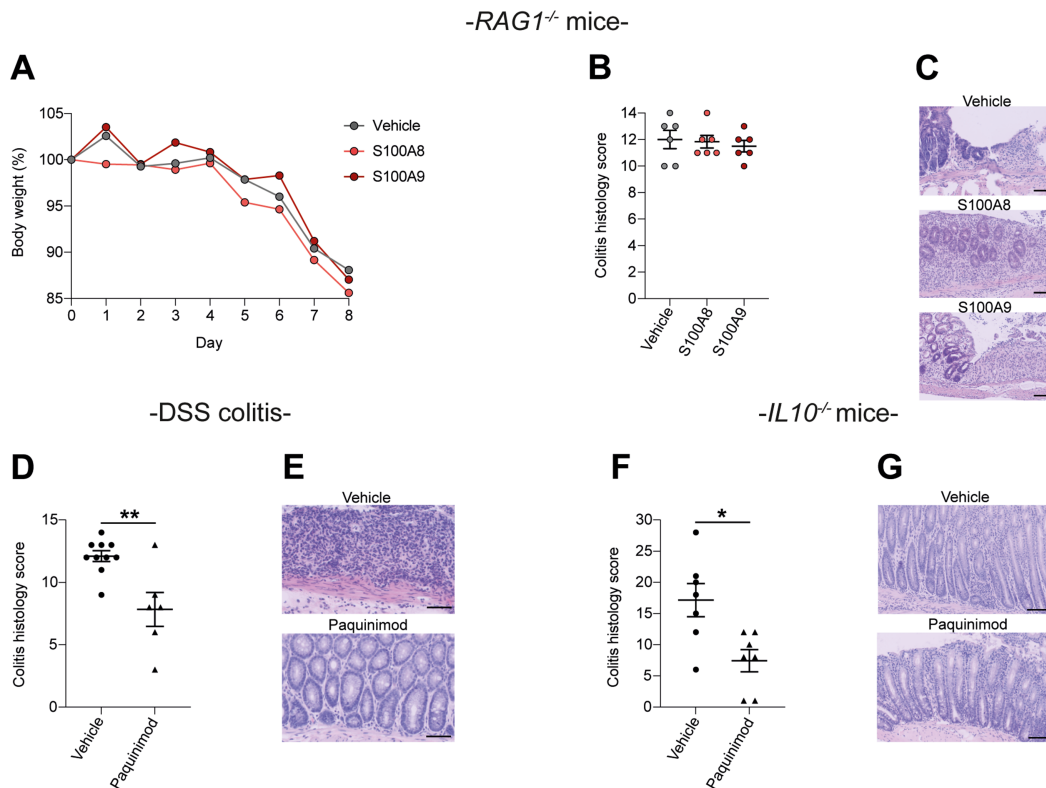


Figure 6. The colitogenic effect of human S100A8 and S100A9 homodimers requires adaptive immunity. (A) Body weight course, (B) colitis histology score, and (C) representative H&E images of $Rag1^{-/-}$ mice exposed to DSS and oral gavage with vehicle, S100A8, or S100A9 ($n = 6/6/6$; 8–9 weeks; mean \pm standard error of the mean [SEM] shown; 1-way analysis of variance [ANOVA] with post hoc Bonferroni). Scale bars, 50 μ m. (D) Colitis histology score and (E) representative H&E images of WT mice exposed to DSS and treated with paquinimod or vehicle ($n = 10/6$; 8–9 weeks; mean \pm SEM shown; two-tailed Student's t -test). Note the shared vehicle group with experiment shown in in Figure 3A–D, as experiments were performed simultaneously. Scale bars, 100 μ m. (F) Colitis histology score and (G) representative H&E images of $Il10^{-/-}$ mice treated with paquinimod or vehicle ($n = 7/7$; 7–8 weeks; mean \pm SEM shown; two-tailed Student's t -test). Scale bars, 100 μ m. * $P < .05$, ** $P < .01$.

Figure 5. Human S100A8 and S100A9 homodimers enhance T-cell activation. (A) Overview of the experimental approach. $CD3^{+}$ and $CD8^{+}$ T cells were isolated by negative selection (see Materials and Methods) and T cells of each healthy donor were cultivated in the presence of interleukin (IL) 2. $CD3^{+}$ T cells were additionally activated with anti-CD3/28. Cells were stimulated with S100A8, S100A9, and S100A8/S100A9 (1:1), while vehicle served as a control. Surface markers were analyzed after 24 hours, and intracellular cytokine staining was performed after 48 hours of stimulation by flow cytometry. Results are normalized to vehicle and depicted as percentage change relative to control. Effector memory T_{EM} were defined as $CD62L^{-}/CD45RO^{+}$, and CD25 and CD69 were used as activation markers. $CD8^{+}$ T cells were additionally analyzed by bulk RNA sequencing and Western blot. FACS, fluorescence-activated cell sorter. Image was created in <https://BioRender.com>. (B and C) Quantification of activated $CD4^{+}$ T cells after stimulation with S100A8, S100A9, and S100A8/S100A9 (1:1) for 24 hours ($n = 6/6/6/6$; Kruskal-Wallis test with Dunn's correction; median shown). (D) Quantification of effector memory $CD4^{+}$ T cells after stimulation with S100A8, S100A9, and S100A8/A9 for 24 hours ($n = 6/6/6/6$; Kruskal-Wallis test with Dunn's correction; median shown). (E and F) Quantification of activated $CD8^{+}$ T cells after stimulation with S100A8, S100A9, and S100A8/S100A9 (1:1) for 24 hours ($n = 6/6/6/6$; Kruskal-Wallis test with Dunn's correction; median shown). (G) Quantification of effector memory $CD8^{+}$ T cells after stimulation with S100A8, S100A9, and S100A8/S100A9 (1:1) for 24 h ($n = 6/6/6/6$; Kruskal-Wallis test with Dunn's correction; median shown). (H) Quantification of intracellular granzyme B (GrzB) in $CD8^{+}$ T cells after stimulation with S100A8, S100A9, and S100A8/S100A9 (1:1) for 48 h ($n = 6/6/6/6$; Kruskal-Wallis test with Dunn's correction; median shown). (I) Quantification of secreted IL17A in the supernatant of $CD3^{+}$ T cells after stimulation with S100A8, S100A9, and S100A8/S100A9 (1:1) for 48 hours ($n = 6/6/6/6$; Kruskal-Wallis test with Dunn's correction; median shown). (J) Heat map showing activity (act) scores (obtained with a multivariate linear model) of pathways in $CD8^{+}$ T cells obtained from healthy individuals treated with vehicle, S100A8, S100A9, or S100A8/S100A9 (1:1). The y-axis indicates treatment condition, the x-axis indicates regulated pathways. Red indicates up-regulation of a pathway relative to vehicle, blue indicates down-regulation. Representative immunoblot of $CD8^{+}$ T cells after S100A8, S100A9 and S100A8/S100A9 (1:1) stimulation for the (K) nuclear factor (NF)- κ B pathway ($n = 6$) and (L) signal transducer and activator of transcription 3 (STAT3) ($n = 7$). EGFR, epidermal growth factor receptor; GAPDH, glyceraldehyde-3-phosphate dehydrogenase; IKK, I κ B kinase; JAK/STAT, Janus kinase/signal transducer and activator of transcription; MAPK, mitogen-activated protein kinase; NF κ B, nuclear factor- κ B; p-, phosphorylated; PI3K, phosphatidylinositol-3-kinase; TGF, transforming growth factor; TNF, tumor necrosis factor; TRAIL, TNF-related apoptosis-inducing ligand; VEGF, vascular endothelial growth factor. * $P < .05$, ** $P < .01$, *** $P < .001$.

We further focused on enhanced CD4⁺ and CD8⁺ T-cell activity, because these pathways have been implicated in the control of chronic gut inflammation in IBD²⁷ and because S100A8 and S100A9 promoted CD4⁺ and CD8⁺ T-cell accumulation during colitis. As such, our study complements previous studies on S100A8 and S100A9 actions during colitis^{28,29} and beyond the intestine, for example in inflammatory liver disorders,³⁰ inflammatory skin disease, and autoimmunity.^{12–15,31}

Our study further expands the knowledge of S100A8 and S100A9 actions in the human intestine of newborns⁹ and may explain how S100A8 and S100A9 shape intestinal immune maturation, as recently studied in malnourished mice.³² We acknowledge that pleiotropic mechanisms may be involved in the immunologic effects of homodimers, for example, previously described Toll-like receptor 4 or receptor for advanced glycation end products activation,^{13,14} which we did not disentangle in our study.

Our study conveys important clinical implications. First, human S100A8 and S100A9 homodimers are not detectable by current clinical fecal CP assays, suggesting a diagnostic gap that could obscure the diagnosis of active IBD in symptomatic patients with low fecal CP (<150 µg/g).

Second, our studies indicate that S100A8 and S100A9 homodimers promote enteritis and colitis in mice, partly by activation of T cells, suggesting that blockade of S100A8 or S100A9 configurations could be used as a strategy to treat IBD.

However, the diagnostic use and therapeutic targeting of S100A8 and S100A9 dimers is limited by several unresolved issues, warranting further investigations. First, our cross-sectional cohorts displayed phenotypic heterogeneity and endoscopy readouts were not available for all cohorts.

Second, the odds to detect clinical disease activity with S100A9 in the discovery cohort was corroborated in a relatively small independent cohort (N = 84), which, however, also indicated an association of S100A9 detection with endoscopic disease activity.

Third, we were unable to identify a clinical phenotype explaining the presence or absence of fecal S100A8 or S100A9 dimers.

To overcome these limitations, large controlled biomarker trials with endoscopy readouts are necessary, which may add clinical value to fecal S100A8 or S100A9 detection in IBD in the future. For instance, recent studies indicated that fecal CP quantification is associated with the probability of clinical, endoscopic, and histologic remission in UC,³³ and a link with heterogenous CD courses has been identified.³⁴

Collectively, our study is notable because it challenges our perception of remission in IBD and specifically the interpretation of low fecal CP concentration in symptomatic IBD patients. Large fecal biomarker trials with endoscopic validation of IBD activity are warranted to determine advantages and disadvantages of fecal S100A9 (or possibly S100A8) dimer detection compared with CP quantification, to guide the use in clinical practice in the future. Beyond the intestine, the clinical utility of S100A9 detection has been suggested by 2 recent studies using patient sera,

which indicated that S100A9 and CP could be a specific biomarker for psoriasis arthritis¹⁶ and that S100A9 could serve as a biomarker for brain metastasis response to radiotherapy.³⁵

Our study provides a new perspective for CP subunits as biomarkers for intestinal inflammation in IBD and possibly other inflammatory conditions of the human intestine. Our experimental findings may pave the way for gut-selective medical therapy targeting S100A9 dimers, which can potentially be tailored to patients with IBD by fecal profiling of CP configurations.

Supplementary Material

Note: To access the supplementary material accompanying this article, visit the online version of *Gastroenterology* at www.gastrojournal.org, and at <https://doi.org/10.1053/j.gastro.2025.08.040>.

References

1. Chang JT. Pathophysiology of inflammatory bowel diseases. *N Engl J Med* 2020;383:2652–2664.
2. GBD 2017 Inflammatory Bowel Disease Collaborators. The global, regional, and national burden of inflammatory bowel disease in 195 countries and territories, 1990–2017: a systematic analysis for the Global Burden of Disease Study 2017. *Lancet Gastroenterol Hepatol* 2020;5:17–30.
3. Le Berre C, Honap S, Peyrin-Biroulet L. Ulcerative colitis. *Lancet* 2023;402:571–584.
4. Dolinger M, Torres J, Vermeire S. Crohn's disease. *Lancet* 2024;403:1177–1191.
5. Turner D, Ricciuto A, Lewis A, et al. STRIDE-II: an update on the Selecting Therapeutic Targets in Inflammatory Bowel Disease (STRIDE) initiative of the International Organization for the Study of IBD (IOIBD): determining therapeutic goals for treat-to-target strategies in IBD. *Gastroenterology* 2021;160:1570–1583.
6. Jukic A, Bakiri L, Wagner EF, et al. Calprotectin: from biomarker to biological function. *Gut* 2021;70:1978–1988.
7. Zhang X, Wei L, Wang J, et al. Suppression colitis and colitis-associated colon cancer by anti-S100a9 antibody in mice. *Front Immunol* 2017;8:1774.
8. Aranda CJ, Ocón B, Arredondo-Amador M, et al. Calprotectin protects against experimental colonic inflammation in mice. *Br J Pharmacol* 2018;175:3797–3812.
9. Willers M, Ulas T, Völger L, et al. S100A8 and S100A9 are important for postnatal development of gut microbiota and immune system in mice and infants. *Gastroenterology* 2020;159:2130–2145.e2135.
10. Odink K, Cerletti N, Brügger J, et al. Two calcium-binding proteins in infiltrate macrophages of rheumatoid arthritis. *Nature* 1987;330:80–82.
11. Pruenster M, Immler R, Roth J, et al. E-selectin-mediated rapid NLRP3 inflammasome activation regulates S100A8/S100A9 release from neutrophils via transient gasdermin D pore formation. *Nat Immunol* 2023;24:2021–2031.

12. Vogl T, Gharibyan AL, Morozova-Roche LA. Pro-inflammatory S100A8 and S100A9 proteins: self-assembly into multifunctional native and amyloid complexes. *Int J Mol Sci* 2012;13:2893–2917.
13. Vogl T, Stratis A, Wixler V, et al. Autoinhibitory regulation of S100A8/S100A9 alarmin activity locally restricts sterile inflammation. *J Clin Invest* 2018;128:1852–1866.
14. Loser K, Vogl T, Voskort M, et al. The Toll-like receptor 4 ligands Mrp8 and Mrp14 are crucial in the development of autoreactive CD8⁺ T cells. *Nat Med* 2010;16:713–717.
15. Schonthaler HB, Guinea-Viniegra J, Wculek SK, et al. S100A8-S100A9 protein complex mediates psoriasis by regulating the expression of complement factor C3. *Immunity* 2013;39:1171–1181.
16. Mellor LF, Gago-Lopez N, Bakiri L, et al. Keratinocyte-derived S100A9 modulates neutrophil infiltration and affects psoriasis-like skin and joint disease. *Ann Rheum Dis* 2022;81:1400–1408.
17. Plattner C, Sturm G, Kühl AA, et al. IBDome: an integrated molecular, histopathological, and clinical atlas of inflammatory bowel diseases. Preprint. *bioRxiv* 2025; 2025:03.26.645544.
18. Imhann F, Van der Velde KJ, Barbieri R, et al. The 1000IBD project: multi-omics data of 1000 inflammatory bowel disease patients; data release 1. *BMC Gastroenterol* 2019;19:5.
19. Mayr L, Grabherr F, Schwärzler J, et al. Dietary lipids fuel GPX4-restricted enteritis resembling Crohn's disease. *Nat Commun* 2020;11:1775.
20. Kaser A, Lee AH, Franke A, et al. XBP1 links ER stress to intestinal inflammation and confers genetic risk for human inflammatory bowel disease. *Cell* 2008;134:743–756.
21. Adolph TE, Tomczak MF, Niederreiter L, et al. Paneth cells as a site of origin for intestinal inflammation. *Nature* 2013;503:272–276.
22. Schwärzler J, Mayr L, Vich Vila A, et al. PUFA-induced metabolic enteritis as a fuel for Crohn's disease. *Gastroenterology* 2022;162:1690–1704.
23. Singh S, Ananthakrishnan AN, Nguyen NH, et al. AGA Clinical Practice Guideline on the Role of Biomarkers for the Management of Ulcerative Colitis. *Gastroenterology* 2023;164:344–372.
24. Corridoni D, Antanaviciute A, Gupta T, et al. Single-cell atlas of colonic CD8(+) T cells in ulcerative colitis. *Nat Med* 2020;26:1480–1490.
25. Martini GR, Tikhonova E, Rosati E, et al. Selection of cross-reactive T cells by commensal and food-derived yeasts drives cytotoxic T(H)1 cell responses in Crohn's disease. *Nat Med* 2023;29:2602–2614.
26. Bacher P, Hohnstein T, Beerbaum E, et al. Human anti-fungal Th17 immunity and pathology rely on cross-reactivity against *Candida albicans*. *Cell* 2019;176:1340–1355.e1315.
27. Neurath MF. Targeting immune cell circuits and trafficking in inflammatory bowel disease. *Nat Immunol* 2019;20:970–979.
28. Fujita Y, Khateb A, Li Y, et al. Regulation of S100A8 stability by RNF5 in intestinal epithelial cells determines intestinal inflammation and severity of colitis. *Cell Rep* 2018;24:3296–3311.e3296.
29. Zhen D, Wang S, Liu Z, et al. Fibroblast growth factor 20 attenuates colitis by restoring impaired intestinal epithelial barrier integrity and modulating macrophage polarization via S100A9 in an NF-kappaB-dependent manner. *Cell Mol Gastroenterol Hepatol* 2025;19:101486.
30. Rodrigues RM, He Y, Hwang S, et al. E-selectin-dependent inflammation and lipolysis in adipose tissue exacerbate steatosis-to-NASH progression via S100A8/9. *Cell Mol Gastroenterol Hepatol* 2022;13:151–171.
31. Palomo-Irigoyen M, Bakiri L, Hendrikx T, et al. Chronic skin and systemic inflammation modulated by S100A8 and S100A9 complexes. *Cell Death Differ* 2025;32:1833–1844.
32. Perruzza L, Heckmann J, Rezzonico Jost T, et al. Post-natal supplementation with alarmins S100a8/a9 ameliorates malnutrition-induced neonate enteropathy in mice. *Nat Commun* 2024;15:8623.
33. Dulai PS, Feagan BG, Sands BE, et al. Prognostic value of fecal calprotectin to inform treat-to-target monitoring in ulcerative colitis. *Clin Gastroenterol Hepatol* 2023;21:456–466.e457.
34. Constantine-Cooke N, Monterrubio-Gómez K, Plevris N, et al. Longitudinal fecal calprotectin profiles characterize disease course heterogeneity in Crohn's disease. *Clin Gastroenterol Hepatol* 2023;21:2918–2927.e2916.
35. Monteiro C, Miarka L, Perea-García M, et al. Stratification of radiosensitive brain metastases based on an actionable S100A9/RAGE resistance mechanism. *Nat Med* 2022;28:752–765.

Received December 3, 2024. Accepted August 28, 2025.

Correspondence

Address correspondence to: Timon E. Adolph, MD, PhD, Department of Internal Medicine I, Gastroenterology, Hepatology, Endocrinology & Metabolism, Medical University of Innsbruck, Anichstraße 35, 6020 Innsbruck, Austria. e-mail: timon-erik.adolph@i-med.ac.at; or Herbert Tilg, MD, Department of Internal Medicine I, Gastroenterology, Hepatology, Endocrinology & Metabolism, Medical University of Innsbruck, Anichstraße 35, 6020 Innsbruck, Austria. e-mail: herbert.tilg@i-med.ac.at.

Acknowledgments

Members of the TRR241 IBDome Consortium include Imke Atraya,¹ Raja Atraya,¹ Petra Bacher,^{2,3} Christoph Becker,¹ Christian Bojarski,⁴ Nathalie Britzen-Laurent,¹ Caroline Bosch-Voskens,¹ Hyun-Dong Chang,⁵ Andreas Diefenbach,⁶ Claudia Günther,¹ Ahmed N. Hegazy,⁴ Kai Hildner,¹ Christoph S.N. Klose,⁶ Kristina Koop,¹ Susanne Krug,⁴ Anja A. Kühl,⁴ Moritz Leppkes,¹ Rocío López-Posadas,¹ Leif S.-H. Ludwig,⁷ Clemens Neufert,¹ Markus Neurath,¹ Jay V. Patankar,¹ Magdalena Prüß,³ Andreas Radbruch,⁵ Chiara Romagnani,³ Francesca Ronchi,⁶ Ashley D. Sanders,^{4,8} Alexander Scheffold,² Jörg-Dieter Schulzke,⁴ Michael Schumann,⁴ Sebastian Schürmann,¹ Britta Siegmund,⁴ Michael Stürzl,¹ Antigoni Triantafylloulopoulou,^{5,9} Maximilian Waldner,¹ Carl Weidinger,⁴ Stefan Wirtz,¹ and Sebastian Zundler¹; from the ¹Department of Medicine I, Friedrich-Alexander University, Erlangen, Germany; ²Institute of Clinical Molecular Biology, Christian-Albrecht University of Kiel, Kiel, Germany; ³Institute of Immunology, Christian-Albrecht University of Kiel and Universitätsklinikum Schleswig-Holstein, Kiel, Germany; ⁴Department of Gastroenterology, Infectious Diseases and Rheumatology, Charité—Universitätsmedizin Berlin, corporate member of Freie Universität Berlin and Humboldt-Universität zu Berlin, Berlin, Germany; ⁵Deutsches Rheuma-Forschungszentrum, ein Institut der Leibniz-Gemeinschaft, Berlin, Germany; ⁶Institute of Microbiology, Infectious Diseases and Immunology Charité—Universitätsmedizin Berlin, corporate member of Freie Universität Berlin and Humboldt-Universität zu Berlin, Berlin, Germany; ⁷Berlin Institute für Gesundheitsforschung, Medizinische System Biologie, Charité—Universitätsmedizin Berlin, Berlin, Germany; ⁸Max Delbrück Center für

Molekulare Medizin, Charité—Universitätsmedizin Berlin, Berlin, Germany; and ⁹Department of Rheumatology and Clinical Immunology, Charité—Universitätsmedizin Berlin, corporate member of Freie Universität Berlin and Humboldt-Universität zu Berlin, Berlin, Germany.

The authors thank Herbert Lindner and Theresia Dunzendorfer-Matt for helpful discussions.

CRedit Authorship Contributions

Almina Jukic, MD, MSc (Conceptualization: Equal; Data curation: Lead; Formal analysis: Lead; Investigation: Lead; Methodology: Lead; Validation: Lead; Visualization: Lead; Writing – original draft: Lead; Writing – review & editing: Lead)

Richard Hilbe, BSc (Data curation: Equal; Formal analysis: Equal; Investigation: Equal; Methodology: Equal; Writing – review & editing: Equal)

Luis Zundel, MSc (Data curation: Equal; Formal analysis: Equal; Methodology: Equal; Writing – original draft: Equal; Writing – review & editing: Equal)

Peter Willeit, MD, PhD (Data curation: Equal; Formal analysis: Equal; Investigation: Equal; Methodology: Equal; Validation: Equal; Writing – original draft: Equal; Writing – review & editing: Equal)

Klaus Faserl, PhD (Data curation: Equal; Formal analysis: Equal; Methodology: Equal; Writing – review & editing: Equal)

Christina Plattner, PhD (Data curation: Equal; Formal analysis: Equal; Methodology: Equal; Visualization: Equal; Writing – review & editing: Equal)

Andreas Zollner, MD, PhD (Data curation: Supporting; Formal analysis: Supporting; Methodology: Supporting; Writing – review & editing: Equal)

Moritz Meyer, MD (Data curation: Equal; Investigation: Equal; Methodology: Equal; Writing – review & editing: Equal)

Kerstin Siegmund, PhD (Conceptualization: Equal; Data curation: Equal; Formal analysis: Equal; Methodology: Equal; Writing – review & editing: Equal)

Victoria Klepsch, PhD (Conceptualization: Equal; Data curation: Equal; Formal analysis: Equal; Methodology: Equal; Writing – review & editing: Equal)

Valentin Marteau, MSc (Data curation: Equal; Formal analysis: Equal; Methodology: Equal; Visualization: Equal; Writing – review & editing: Equal)

Arnau Vich Vila, PhD (Data curation: Equal; Formal analysis: Equal; Methodology: Equal; Resources: Equal; Validation: Equal; Writing – review & editing: Equal)

Julian Schwärzler, MD, PhD (Data curation: Supporting; Formal analysis: Supporting; Methodology: Supporting; Writing – review & editing: Supporting)

Kathrin Vouk, MD, BSc (Data curation: Equal; Methodology: Equal; Writing – review & editing: Equal)

Anna Kozsar, MD (Data curation: Equal; Methodology: Equal)

Dietmar Rieder, PhD (Data curation: Equal; Formal analysis: Equal; Methodology: Equal; Visualization: Equal; Writing – review & editing: Equal)

Amos Weichberger, MD (Data curation: Equal; Methodology: Equal; Writing – review & editing: Equal)

Bettina Sarg, PhD (Conceptualization: Supporting; Data curation: Supporting; Methodology: Supporting; Writing – review & editing: Supporting)

Felix Grabherr, MD, PhD (Data curation: Supporting; Methodology: Supporting)

Lisa Mayr, PhD (Data curation: Supporting; Methodology: Supporting)

Patrizia Moser, MD (Resources: Equal)

Niloofer Nemati, PhD (Methodology: Supporting)

Sabine Scholl-Bürgi, MD (Methodology: Supporting; Resources: Equal)

Daniela Karall, MD (Methodology: Supporting)

Georg F. Vogel, MD, PhD (Data curation: Supporting; Methodology: Supporting; Resources: Equal)

Lina Welz, MD (Data curation: Supporting; Resources: Supporting)

Denise Aldrian, MD (Resources: Supporting)

Robert Koch, MD (Resources: Equal)

Alexandra Pfister, BSc (Data curation: Supporting; Investigation: Supporting; Methodology: Supporting)

Qitao Ran, PhD (Methodology: Equal; Resources: Equal)

Arthur Kaser, MD (Methodology: Equal; Resources: Equal)

Richard S. Blumberg, MD (Methodology: Equal; Resources: Equal)

Ivan Tancevski, MD, PhD (Methodology: Supporting; Resources: Supporting)

Felix Sommer, PhD (Data curation: Equal; Formal analysis: Equal; Methodology: Equal; Writing – review & editing: Equal)

Petra Bacher, PhD (Formal analysis: Equal; Methodology: Equal; Resources: Equal)

Stefan Schreiber, MD (Resources: Equal)

Philip Rosenstiel, MD (Methodology: Supporting; Resources: Equal; Writing – review & editing: Equal)

Konrad Aden, MD (Methodology: Supporting; Resources: Equal; Writing – review & editing: Equal)

Gottfried Baier, PhD (Conceptualization: Equal; Methodology: Equal; Resources: Equal)

Latifa Bakiri, PhD (Conceptualization: Supporting; Resources: Equal; Writing – review & editing: Equal)

Thomas Müller, MD (Resources: Equal)

Günter Weiss, MD (Resources: Equal)

TRR241 IBDome Consortium (Resources: Equal)

Rinse K. Weersma, MD (Data curation: Equal; Formal analysis: Equal; Resources: Equal; Writing – review & editing: Equal)

Zlatko Trajanoski, PhD (Methodology: Equal; Resources: Equal)

Erwin F. Wagner, PhD (Conceptualization: Supporting; Investigation: Supporting; Resources: Equal; Writing – review & editing: Equal)

Herbert Tilg, MD (Conceptualization: Lead; Funding acquisition: Lead; Investigation: Lead; Project administration: Lead; Resources: Lead; Supervision: Lead; Writing – original draft: Lead; Writing – review & editing: Lead)

Timon Erik Adolph, MD, PhD (Conceptualization: Lead; Formal analysis: Lead; Funding acquisition: Lead; Investigation: Lead; Project administration: Lead; Resources: Lead; Supervision: Lead; Writing – original draft: Lead; Writing – review & editing: Lead)

Writing – review & editing: Lead)

Writing – review & editing: Lead)

Writing – review & editing: Lead)

Writing – review & editing: Lead)

Writing – review & editing: Lead)

Writing – review & editing: Lead)

Writing – review & editing: Lead)

Writing – review & editing: Lead)

Writing – review & editing: Lead)

Writing – review & editing: Lead)

Writing – review & editing: Lead)

Writing – review & editing: Lead)

Writing – review & editing: Lead)

Writing – review & editing: Lead)

Writing – review & editing: Lead)

Writing – review & editing: Lead)

Writing – review & editing: Lead)

Writing – review & editing: Lead)

Writing – review & editing: Lead)

Writing – review & editing: Lead)

Writing – review & editing: Lead)

Writing – review & editing: Lead)

Writing – review & editing: Lead)

Writing – review & editing: Lead)

Writing – review & editing: Lead)

Writing – review & editing: Lead)

Writing – review & editing: Lead)

Writing – review & editing: Lead)

Writing – review & editing: Lead)

Writing – review & editing: Lead)

Writing – review & editing: Lead)

Writing – review & editing: Lead)

Writing – review & editing: Lead)

Writing – review & editing: Lead)

Writing – review & editing: Lead)

Writing – review & editing: Lead)

Writing – review & editing: Lead)

Writing – review & editing: Lead)

Writing – review & editing: Lead)

Writing – review & editing: Lead)

Writing – review & editing: Lead)

Writing – review & editing: Lead)

Writing – review & editing: Lead)

Writing – review & editing: Lead)

Writing – review & editing: Lead)

Writing – review & editing: Lead)

Writing – review & editing: Lead)

Writing – review & editing: Lead)

Writing – review & editing: Lead)

Writing – review & editing: Lead)

Writing – review & editing: Lead)

Writing – review & editing: Lead)

Writing – review & editing: Lead)

Writing – review & editing: Lead)

Writing – review & editing: Lead)

Writing – review & editing: Lead)

Writing – review & editing: Lead)

Writing – review & editing: Lead)

Writing – review & editing: Lead)

Writing – review & editing: Lead)

Writing – review & editing: Lead)

Writing – review & editing: Lead)

Writing – review & editing: Lead)

Writing – review & editing: Lead)

Writing – review & editing: Lead)

Writing – review & editing: Lead)

Writing – review & editing: Lead)

Writing – review & editing: Lead)

Supplemental information

Fecal Detection of Calprotectin Subunits Links Inflammatory Bowel Disease Activity With Chronicity of Intestinal Inflammation

Almina Jukic, Richard Hilbe, Luis Zundel, Peter Willeit, Klaus Faserl, Christina Plattner, Andreas Zollner, Moritz Meyer, Kerstin Siegmund, Victoria Klepsch, Valentin Marteau, Arnau Vich Vila, Julian Schwärzler, Kathrin Vouk, Anna Kozsar, Dietmar Rieder, Amos Weichberger, Bettina Sarg, Felix Grabherr, Lisa Mayr, Patrizia Moser, Niloofar Nemati, Sabine Scholl-Bürgi, Daniela Karall, Georg F. Vogel, Lina Welz, Denise Aldrian, Robert Koch, Alexandra Pfister, Qitao Ran, Arthur Kaser, Richard S. Blumberg, Ivan Tancevski, Felix Sommer, Petra Bacher, Stefan Schreiber, Philip Rosenstiel, Konrad Aden, Gottfried Baier, Latifa Bakiri, Thomas Müller, Günter Weiss, TRR241 IBDome Consortium Rinse K. Weersma, Zlatko Trajanoski, Erwin F. Wagner, Herbert Tilg, and Timon E. Adolph

Supplementary Information

Supplemental Materials and Methods

S1008 and S100A9 homodimer quantification in stool

Stool samples were diluted 1:10 (w/v) in ice-cold PBS containing EDTA-free protease and phosphatase inhibitors (Thermo Fisher Scientific, 78443). Specimens were vortexed for 30 sec and incubated on a tube rotator at room temperature for 25 min. Homogenates were vortexed for 30 sec and then centrifuged at 10,000 rpm for 20 min. Supernatants were collected and centrifuged for 15 min at 15,000 g and 4°C. Supernatant was stored at -80°C until analysis by ELISA. The following ELISAs were used for human fecal studies: S100A8 (R&D, DY4570-05), S100A9 (R&D, DY5578), S100A8/S100A9 (R&D, DY8226-05), S100A8/A9 (Eurospital Diagnostic, 9031). The following clinically established calprotectin assays were tested for their specificity to detect S100A8 or S100A9: S100A8/A9 (BÜHLMANN, K181012); S100A8/A9 (Euroimmun, EQ 6831-9601 W); S100A8/A9 (Eurospital Diagnostic, 9031); S100A8/A9 (Eurospital Diagnostic, 9300).

S100A8 and S100A9 protein interactors in human stool

Co-immunoprecipitation was performed to identify protein–protein interactions by using S100A8- and S100A9-specific antibodies to indirectly capture interaction partners of both target proteins. Per sample 250 µg of Pierce Magnetic Beads (Thermo Fisher Scientific, 88816) were transferred to a 1.5 mL low protein binding tube (Thermo Scientific, 90410) and separated on a magnetic rack. Beads were washed with PBS containing 0.1% CHAPS (ROTH, 1479.1) at pH 7.4 by shaking the tube thoroughly for 30 sec. Washing was repeated five times. Beads were then incubated with 6 µg of S100A8 (abcam, ab92331) or S100A9 (cell signaling, 72590S) antibody dissolved in 1 mL of incubation buffer (PBS containing 0.1% CHAPS, 0.1% Tween and 1% BSA at pH 7.4) on a rotator at 40 rpm and RT for 2 h. Samples were then washed five times to remove any remains of unconjugated antibodies. Washed beads were incubated with 80 µl of stool supernatant or vehicle diluted in 920 µl of binding buffer (PBS containing 0.1% CHAPS and 0.2 pmol protease inhibitors at pH 7.4) on a rotator at 40 rpm and RT for 1 h. Samples were then incubated overnight on a rotator at 40 rpm at 4°C. Beads were washed five times, resuspended in 200 µL of 1% formic acid (Fisher Chemical, A117-05AMP), vortexed and

incubated at RT for 5 min. Samples were separated on a magnetic rack, supernatants were collected, lyophilized and dissolved in 100 μ l twice-distilled water for LC-MS/MS analysis.

Expression and purification of human recombinant S100A8 and S100A9

Plasmid assembly of human recombinant S100A8 and S100A9: Human S100A9 (AA 1-114) and human S100A8 (AA 1-93) were ordered as gBlocks from idtDNA and integrated into the linearized bacterial expression vector pET28a (Novagen, 69866-3) at equimolar concentrations by gibson assembly (NEBuilder® HiFi DNA Assembly Master Mix, E2621S). Expression in the pET28a system is controlled by a T7 promoter that is active only when the plasmid is paired with an appropriate bacterial host that can express the viral T7 polymerase. The pET28a-hS100A9 plasmid and the pET28a-hS100A8 plasmid were separately introduced into chemically competent KRX cells (Promega, L3002) that express T7 polymerase controlled by a rhamnose inducible promoter (rhaBAD). In contrast to recombinant hS100A9 protein, recombinant hS100A8 was predominantly found in insoluble inclusion bodies and remaining hS100A8 was prone to aggregation. This was counteracted by inserting a short (7.6 kDA) N' terminal fusion tag (FH8) to S100A8, which enhanced solubility and stability. Purification was improved by introducing an additional 6xHIS tag preceding FH8. Furthermore, a TEV cleavage site was introduced between fusion tag and hS100A8 to enable protein cleavage. The optimized gBlock was induced in the linearized bacterial expression vector pET28a and resulted in the final pET28a-6xHIS-FH8-hS100A8 (AA 2-93) expression plasmid.

Expression: Transformed bacteria were transferred into terrific broth containing 50 μ g mL⁻¹ kanamycin and incubated on a rotation incubator at 250 rpm and 37°C O/N. Overnight cultures (10 mL) were diluted 1:20 in terrific broth containing 50 μ g mL⁻¹ kanamycin and incubated on a rotation incubator at 250 rpm and 37°C until an OD₆₀₀ of 1 was reached. Protein expression was induced by supplementing the medium with 1 mL of 20% rhamnose (w/v) and 200 μ l 1M IPTG. Cultures were incubated at 250 rpm and 25°C for 25 h and bacteria were harvested via centrifugation at 6000 g and 4°C for 10 min. The supernatants were discarded and cell pellets were stored at -20°C until further preparation. Cell lysis and extraction: Bacteria were lysed according to manufacturer's instructions (NZYtech, MB17802). Briefly, cells were resuspended in 5 mL of NZY Bacterial Cell Lysis Buffer

(containing 10 mg mL⁻¹ lysozyme, 250 mg mL⁻¹ DNase I and 1x EDTA-free protease inhibitors) per gram cell paste and incubated on a tube rotator for 25 min at RT. Proteins were harvested through centrifugation for 15 min at 15,000 g and 4°C. The collected supernatants contained recombinant human S100A8 and S100A9. Purification of recombinant human S100A9: S100A9 protein was purified through anion-exchange chromatography using an ÄKTA purification system. The sample was diluted to 500 mL with buffer consisting of 50 mM TRIS at pH 7.5, 10 mM NaCl, 1 g L⁻¹ colistin and 2.5 mM beta-mercaptoethanol and loaded at 5 mL min⁻¹ onto an equilibrated 5 mL HiTrap CaptoQ ImpRes column (Cytiva, 17547055). Unbound proteins were washed from the column using AIEX Running Buffer (50 mM Tris pH 7.5 at 25°C, 50 mM NaCl and 0.001% Pluronic F68). Elution of recombinant S100A9 was performed with AIEX Elution Buffer (5 mM Tris pH 7.5 at 25°C, 1 M NaCl and 0.001% Pluronic F68) at a concentration of 30% with 10CV at a flow rate of 1 mL min⁻¹. Elution fractions of 1 mL were collected in a 96-well master block and analysed. Fractions specific for human S100A9 were collected, pooled and purified using immobilized metal ion affinity chromatography (IMAC). For this purpose, two columns of 1 mL HisTrap excel were run in tandem to achieve the necessary protein binding capacity. The sample was diluted 1:2 with IMAC Running Buffer (25 mM Hepes pH 7.5 at 25°C, 0.5 M NaCl, 5 mM imidazole and 0.001% Pluronic F68) and loaded onto the equilibrated columns. After a 5CV washing step with running buffer, S100A9 was eluted with 5% IMAC Elution Buffer (1 M imidazole pH 7.5 at 25°C, 0.5 M NaCl and 0.001% Pluronic F68) in 15CV.

Purification of recombinant S100A8 protein: S100A8 protein was purified based on its His-FH8 tag using immobilized metal ion affinity chromatography. The sample was diluted to 250 mL in buffer containing 50 mM Hepes pH 7.5, 0.4 M NaCl, 2.5 mM imidazole and 1 g L⁻¹ colistin. The solution was loaded at 2 mL min⁻¹ onto 1 mL HisTrap excel columns (Cytiva, 17371205) run in tandem. Unbound proteins were washed first with 7.5 CV IMAC Running Buffer and second with 5 CV 2% IMAC Elution Buffer. Elution was performed using 15% elution buffer at a flow rate of 1 mL min⁻¹ with 15CV. Elution fractions of 1 mL were collected and analyzed. TEV cleavage: TEV protease was incubated with FH8-S100A8 protein at a concentration of 1U µg⁻¹ protein for 48 h at 4°C. The cleaved S100A8 was recovered by absorption of the FH8 tag and the TEV protease onto PureCube Ni-INDIGO MagBeads (Cube Biotech, 75205). The remaining supernatant contained the cleaved S100A8 protein.

Quality testing and protein storage: Purity of proteins was assessed with Coomassie gel and LC-MS/MS analysis. Protein constitution was validated through size-exclusion chromatography. After quality testing, proteins were concentrated and dissolved in ice-cold PBS using a 10 kDa molecular weight cut-off spin filter. Samples were concentrated a minimum of five times at 3000 g and 4°C. Proteins were sterile filtered through a 0.22 µm membrane and concentrations were determined using Protein Assay (Bio-Rad Laboratories, 5000006). Recombinant proteins were stored in PBS containing 0.1 % BSA at a concentration of 0.5 µg µl⁻¹ at –80°C. Endotoxin levels within recombinant human S100A8 and S100A9 were assessed using the Pierce LAL Chromogenic Endotoxin Quantitation Kit. Testing was performed according to the manufacturer's instructions (Thermo Scientific, A39552).

Size-exclusion chromatography

Recombinant proteins: For the assessment of complex formation and hydrodynamic radius of the purified proteins we used the ÄktaGO system and a Superdex75 10/300 GL increase column (Cytiva, 29148721) calibrated with the LMW Calibration Kit (Cytiva, 28403841).

Purified S100A9 and/or S100A8 proteins were diluted in running buffer (150 mM NaCl, 25 mM Hepes pH 7.5 at 25°C, 0.05% Pluronic F68) and loaded in a 100 µl injection loop according to manufacturer's specifications (Cytiva). To counteract the propensity of S100 proteins to aggregate during chromatographic separation, 0.75 M guanidium chloride (Sigma, G3272-100G) was supplemented in the injected volume. Heterotetramer and heterodimer formation of S100A8 and S100A9 proteins was achieved with a preceding 1 h pre-incubation in the presence of 10 mM CaCl₂.

Stool samples: Fecal samples were prepared as previously described. Apart from the utilized buffers, the procedure was identical to separation of the recombinant S100 proteins. Calibration with the LMW showed a negligible difference between the two buffer systems. PBS was used as running buffer.

Liquid chromatography and tandem mass spectrometry

Sample preparation: Samples in formic acid were lyophilized and re-dissolved in 45 µl of ABC buffer (100mM ammonium bicarbonate, pH 8.0). Proteins were reduced with 5 µl of dithiothreitol (100mM in ABC buffer) at 56°C for 30 min, digested with 0.5 µg of trypsin (Promega, V5111) for 6 h at 37°C, and

alkylated with 50 μ l of iodoacetamide (55mM in ABC buffer) for 20 min at RT. Resulting peptides were lyophilized to a volume of 10 μ l and stored at -20°C until analysis. Liquid chromatography coupled to mass spectrometry (nanoLC-MS/MS): Peptide digests were analyzed using an UltiMate 3000 nano-HPLC system coupled to a Q Exactive Plus Mass Spectrometer (Thermo Scientific) as described previously. Peptides were separated on a 17 cm long column (100 μ m i.d.) packed with 2.4 μ m C18 material (Reprosil). Solvents for nano-HPLC were 0.1% formic acid and 0.1% formic acid in 85% acetonitrile. Total gradient time was 82 min at a flow rate of 300 nL min⁻¹. The 20 most abundant peptides in the full MS scan were selected for MS fragmentation. Isolation window was set to 1.6 m/z . Full scan spectra were acquired from 300 to 1750 m/z at a resolution of 60 000. Peptides were fragmented by HCD with a normalized collision energy set to 28 and scanned at a resolution of 30 000. Database search: The MS data files were processed using Proteome Discoverer, version 2.2 (Thermo Scientific) in combination with the Sequest HT search engine. MS/MS spectra were searched against the Uniprot human reference proteome database with the following search parameters: Enzyme specificity was set to trypsin with two missed cleavages being allowed. Variable modifications were carbamidomethyl on cysteine, oxidation of methionine and acetylation and/or methionine loss of protein N-termini. Precursor mass tolerance was set to 10 ppm; fragment mass tolerance was 20 mmu. Maximum false discovery rate (FDR) for protein and peptide identification was set to 1%. For label-free quantification the Minora Feature Detector node was set to high confidence PSM (peptide spectrum matches) only with at least two isotopic peaks present in the isotope pattern. Retention time alignment was performed at a maximum retention time shift of 10 min and a mass tolerance of 10 ppm. For hypothesis testing, p values were calculated by applying ANOVA (background-based) with Tukey HSD post hoc analysis.

Quantification of S100A8 and S100A9 by LC-MS/MS

For absolute quantification of S100A8 and S100A9, samples were digested equally as described above. Resulting peptides were desalted using Pierce™ C18 pipet tips (Thermo Scientific, 87784), lyophilized and re-solubilized in 32 μ l of 0.1% formic acid. To each sample 8 μ l of two heavy lysine- (13C15N) labeled standard peptides (Thermo Scientific) was added to obtain final concentrations of 0.272 fmol

μl^{-1} and 0.312 fmol μl^{-1} for LGHPDTLNQGEF(K) (S100A9) and ALNSIIDVYH(K) (S100A8), respectively. Each sample was quartered into 10 μl aliquots, three of which were analyzed.

The peptides were separated by nanoLC as described above. The gradient profile was: 0–2 min, 4% B; 2–20 min, 4%–50% B; 20–25 min, 50%–100% B, and 25–30 min, 100% B. The flow rate was 250 nL min⁻¹. For MS analysis, an Orbitrap Eclipse Tribrid mass spectrometer (Thermo Scientific) was operated in data-independent and data-dependent acquisition mode in parallel: full scan spectra were acquired at a resolution of 15000 (at $m/z = 200$) using a scan range of $m/z = 375$ -1500. Automatic gain control target was set to 4e5 with a maximum ionization time of 22 ms. For data-dependent acquisition, low resolution fragment scans of the five most abundant peptides were acquired in the linear ion trap. In parallel data-independent MS/MS acquisition of 17 ions was performed in the orbitrap at a resolution of 15000, normalized target of 200% and maximum ionization time of 22 ms. Isolation window was set to 1.2 Da. Higher-energy collisional dissociation (HCD) was used for both modes of MS/MS acquisition.

Of the 17 ions acquired in data-independent acquisition mode four ions were used for absolute quantification of the two proteins S100-A9 and S100-A8 (endogenous and heavy labeled peptides LGHPDTLNQGEF(K) and ALNSIIDVYH(K), respectively) and another 13 ions were used to evaluate N- or C-terminal protein degradation (Supplementary Table 8).

The MS data files were processed using Skyline 23.1.0.380 (University of Washington). To benchmark the quantitative assay recombinant S100-A8 and S100-A9 were digested and analyzed at concentrations ranging from 53 amol to 10.6 fmol and from 35 amol to 6.9 fmol and on-column, respectively.

Enteritis and colitis assessment

Histology of gut tissue was evaluated on formalin-fixed, paraffin-embedded and hematoxylin- and eosin-stained sections. Disease severity was determined with a semi-quantitative histology scoring by an expert pathologist blinded to sample identity. The histology score for enteritis and colitis is composed of five histological subscores, and was applied as previously reported ^{1,2}.

Immune cell phenotyping

Lamina propria mononuclear cell (LPMC) isolation was initiated by flushing the small intestine multiple times with ice-cold PBS. A 2 cm piece of small intestine was collected, cut into smaller pieces and incubated in IMDM (Gibco, 21056-023) containing 20% FCS, 10 U mL⁻¹ DNase II (Sigma, D8764) and 128 U mL⁻¹ collagenase (Sigma, C1889) on a shaker at 37°C for 1 h. Cells were passed through a 70 µm cell strainer, washed with PBS and filtered through a 40 µm cell strainer. After an additional wash, cells were dissolved in FACS buffer (PBS containing 2 mM EDTA and 2% FCS) and stained for innate or adaptive immune cell populations, as previously described¹. Antibodies were diluted 1:200 in FACS buffer and samples were incubated at 4°C for 30 min. Cells were washed and resuspended in FACS buffer. Analysis was performed on a Cytotflex S (Beckman Coulter). DAPI was used as viability stain and singlets were identified by comparing FSC width and FSC area. The gating strategy for the innate immune cell panel is illustrated in Supplementary Figure 4B. All innate immune cells were defined as CD45⁺, CD3⁻, CD19⁻, CD49b⁻, and DAPI-negative. The gating strategy for the adaptive immune cell panel is depicted in Supplementary Figure 4C. Adaptive immune cells were identified as CD45⁺, CD11c⁻, F4/80⁻, GR1⁻, and DAPI-negative. Following antibodies were used: MERTK-PE/CY7 (eBioscience, 25-5751-82), CD11b-APC/Cy7 (eBioscience, 47-0112-80), CD45-FITC (eBioscience, 11-0454-82), Ly6G-superbright600 (eBioscience, 63-9668-82), MHCII-AF700 (eBioscience, 56-5321-82), DAPI (Biolegend, 422801), CD3-superbright600 (eBioscience, 63-0031-82), CD4-APC/eFluor 780 (eBioscience, 47-0041-82), CD19-PE/CY7 (Biolegend, 115520), CD8-FITC (Bioscience, 553030), CD11c-eFluor450 (eBioscience, 48-0114-82), F4/80-eFluor450 (eBioscience, 48-4801-82), CD11b-Percp (Biolegend, 101229), NK1.1-PE (Biolegend, 108707), SiglecF (CD170) eF660 (eBioscience, 50-1702-80).

Human T cell phenotyping

Human T cell purification, culture and stimulation: PBMCs were isolated from peripheral blood using Ficoll density gradient centrifugation. Blood was diluted in a ratio of 2:1 in PBS and carefully transferred onto 15 mL Lymphoprep (Serumwerk Bernburg, 1858). Samples were centrifuged with slow acceleration and without breaks for 20 min at 200 g and RT. Blood plasma and thrombocytes were

discarded and samples were centrifuged for 20 min at 460 g and RT. Separated PBMCs were collected, filled with PBS to 50 mL and centrifuged for 15 min at 300 g and RT. Pellet was resuspended, washed with PBS and centrifuged for 10 min at 300 g and RT. Washing was repeated twice and the pellet was appropriately resuspended in PBS. Cell number was determined prior to negative selection of CD3⁺ or CD8⁺ T cells according to the user manual (Miltenyi Biotec, 130-096-535, 130-096-495). Briefly, PBMCs were pelleted for 5 min at 300 g and RT, resuspended in MACS buffer containing the respective biotin antibody cocktail and incubated for 5 min at 4°C. Next, MicroBeads were added, and cells were incubated for 10 min at 4°C. Samples were loaded onto a MACS column (Miltenyi Biotec, 130-042-401) and separated in the magnetic field of a MACS Separator (Miltenyi Biotec). Flow-through contained the enriched CD3⁺ or CD8⁺ T cell fractions. Cells were counted, resuspended in T cell medium supplemented with 10 ng mL⁻¹ IL-2 (Peprotech, 200-02) and seeded in a density appropriate for downstream experiments. In case of CD3⁺ T cells (used for flow cytometric and Bio-Plex analyses), stimulation was performed with anti-CD3 (2 µg mL⁻¹ plate bound; BioXcell, BE0001-2) and anti-CD28 (2 µg mL⁻¹ soluble; BioXcell, BE0248) antibodies. FACS analysis: 500,000 CD3⁺ T cells per well of a 96-well plate were seeded. Medium was supplemented with 10 ng mL⁻¹ of IL-2 (Peprotech, 200-02). Co-stimulation was performed with 2 µg mL⁻¹ of anti-CD28 (BioXcell, BE0248) and 1 µg mL⁻¹ soluble anti-CD3 (BioXcell, BE0001-2). T cells were cultivated in the presence of human S100A8 (10 µg mL⁻¹), human S100A9 (10 µg mL⁻¹), human S100A8/A9 (10 µg mL⁻¹) or vehicle for 24 h at 37°C (surface markers) or for 48 h (cytokines). Samples were harvested and FACS staining was performed. For surface FACS analysis 1/5 of the sample was transferred to a 96-well round bottom plate and supplemented with 160 µl HBSS (PanBiotech, P04-32505) per well. Samples were centrifuged for 2 min at 2000 rpm and 4°C. Supernatants were discarded, cells were incubated in antibody solution at 4°C for 20 min. Cells were washed and resuspended in MACS Buffer (PBS containing 0.5% BSA and 2 mM EDTA).

For intracellular staining, cells were treated with GolgiStop (BD, 554724) and GolgiPlug (BD, 555029) for 4 h; 4/5 of the sample was transferred to a 96-well round bottom plate and centrifuged for 2 min at 2000 rpm and 4°C. Supernatants were collected for Bio-Plex analysis, cells were washed with 100 µl HBSS and centrifuged for 2 min at 2000 rpm and 4°C. Samples were stained with 100 µl of BD

Horizon™ Fixable Viability Stain 780 (BD Horizon, 565388), diluted 1:2000 in HBSS, and incubated in the dark for 10 min at RT. Cells were washed with MACS Buffer, resuspended in 160 µl fixation buffer (Biolegend, 420801), and incubated in the dark for 20 min at RT. Samples were centrifuged and resuspended in 200 µl MACS Buffer for overnight storage in the dark at 4°C. Cells were centrifuged and washed with 160 µl 1x Perm/Wash Buffer (diluted Intracellular Staining Permeabilization Wash Buffer (Biolegend, 421002)). Samples were incubated in antibody solution (Perm/Wash Buffer) in the dark for 20 min at RT. Cells were washed and resuspended in MACS Buffer. Samples were measured with a BD FACSCanto II using the FACS Diva software. Acquired data were analyzed using FlowJo software.

Following antibodies were used: CD25-PerCP-Cyanine 5.5 (Biolegend, 356111); CD45RO-Fluor® 488 (Biolegend, 304212), CD4-Pacific Blue (Biolegend, 317423); CD62L-PE (Biolegend, 304805), CD69-Alexa Fluor® 647 (Biolegend, 310918); CD8a-Brilliant Violet 510 (Biolegend, 301047), granzyme B-FITC (Biolegend, 515403).

Antigen-reactive T cell enrichment (ARTE)

Peripheral Blood Mononuclear Cells (PBMCs) were freshly isolated from EDTA blood by density gradient centrifugation (Biocoll, Biochrom) on the day of blood donation. ARTE was performed as similarly described^{3,4}. In brief, $1-2.5 \times 10^7$ PBMCs were plated in RPMI-1640 medium (Gibco), supplemented with 5% (v/v) human AB serum (Sigma-Aldrich) in 12-well cell culture plates (1-2 x 10^7 PBMCs each well) or 6-well cell culture plates (more than 2 x 10^7 PBMCs per well). PBMCs were stimulated for 7 h with S100A8, S100A9 and S100A8/9 in the presence of 1 µg mL⁻¹ of CD40 pure antibody (Miltenyi Biotec). For the last 2 h, 1 µg mL⁻¹ of Brefeldin A (Sigma-Aldrich) was added. To multiplex the specificities against S100A8, S100A9 and S100A8/9, the differentially stimulated cells were labeled with different concentrations of two CD4 antibody clones (CD4-BV421, BioLegend, clone OKT4, titer 1:20 and 1:200; CD4-APC-Vio770, Miltenyi Biotec, clone M-T466, titers 1:50 and 1:500). For lower concentrations, the respective unconjugated CD4 pure antibody was added at a concentration of 1 µg mL⁻¹ to block intermixing of the barcode label³. Barcoded populations were pooled and labeled with CD154-biotin followed by Anti-Biotin MicroBeads (CD154 MicroBead Kit,

Miltenyi Biotec) and magnetically enriched with two sequential MS Columns (Miltenyi Biotec). Staining with fluorochrome-conjugated antibodies was performed on the first column, followed by fixation and intracellular staining on the second column. Frequencies of antigen-specific T cells were determined based on the cell count of CD154⁺ T cells after enrichment, normalized to the total number of CD4⁺ T cells applied on the column. For each stimulation, CD154⁺ background cells enriched from the non-stimulated control were subtracted.

Following antibodies were used: CD4-BV421 (clone: OKT4) (Biolegend), CD4-APC-Vio770 (clone: M-T466) (Miltenyi Biotec), CD154-FITC (clone: REA238), CD45RA-PE-Cy5 (clone: HI100), IFN γ -BV785 (clone: 4S.B3).

Cell culture and stimulation

MODE-K, defined as murine immortalized small intestinal epithelial cells (IECs), were kindly provided by D. Kaiserlian. IECs were cultured in high-glucose DMEM (Lonza, BE12-604F) containing 10% FCS (Biochrom, S0115), 10 mM HEPES (Biochrom, L1613), 0.1 mM non-essential amino acids (Gibco, 11140-035), 100 μ g mL⁻¹ streptomycin and 100 U mL⁻¹ penicillin (Biochrom, A2213). Human T cells were isolated from healthy volunteers and cultured in RPMI-1640 (PAN Biotech, P04-18500) containing 10% FCS, 0.1 mM non-essential amino acids, 1 mM sodium pyruvate (Sigma, S8636), 5 mM HEPES buffer, 100 μ g mL⁻¹ streptomycin, 100 U mL⁻¹ penicillin, 2 mM L-glutamine (Biowest, X0550) and 0.01 % mM beta-mercaptoethanol (Sigma Aldrich, 63689). MODE-K IECs were stimulated with human S100A8 (5 μ g mL⁻¹), human S100A9 (5 μ g mL⁻¹), human S100A8/A9 (5 μ g mL⁻¹) or vehicle for 1 h, 8 h, 12 h or 24 h. T cells were stimulated with human S100A8 (10 μ g mL⁻¹), human S100A9 (10 μ g mL⁻¹), human S100A8/A9 (10 μ g mL⁻¹) or vehicle for 1 h, 4 h, 24 h or 48 h.

Generation and stimulation of human colonic epithelial organoids: Biopsy samples from healthy volunteers were collected during screening colonoscopies after informed consent was obtained. Resected tissues were washed with ice-cold PBS, minced into smaller pieces and incubated in Gentle Cell Dissociation Reagent (Stemcell Technologies, 100-0485) on a rocking platform for 30 min at 4°C. Samples were then centrifuged for 5 min at 290 g and 4°C. Pellets were resuspended in ice-cold DMEM containing 1% BSA and strained through a 70 μ m filter. Crypts were counted and seeded within 50 μ l

of Matrigel (BD, 356231) on a pre-warmed 24-well plate. Matrigel was solidified at 37°C for 10 min and samples were then incubated with 500 µl IntestiCult Growth Medium (Stemcell Technologies, 06010) containing 100 µg mL⁻¹ streptomycin and 100 U mL⁻¹ penicillin at 37°C with 5% CO₂. Medium was changed at an interval of three days and organoids were split in a ratio of 1:6 every seven days. For single-cell RNA sequencing experiments, organoids were cultivated as monolayers according to manufacturer's instructions (Stemcell Technologies). Briefly, organoids were collected, dissolved in 1 mL Gentle Cell Dissociation Reagent and incubated for 10 min at RT. Dissociated organoids were centrifuged for 5 min at 290 g. Pellets were washed with DMEM/F-12 (Gibco, 12634-010) and centrifuged again for 5 min at 290 g. Samples were resuspended in 1 mL of 0.05 % trypsin-EDTA (Gibco, 25300-054) for 10 min at 37°C. Cells were seeded in 96-well plates coated with 5% Matrigel in IntestiCult Growth Medium and incubated with 200 µl IntestiCult™ Organoid Differentiation Medium (Stemcell Technologies, 100-0214) containing 10 µM Y-27632 (dihydrochloride) (Stemcell, 72304), 100 µg mL⁻¹ streptomycin and 100 U mL⁻¹ penicillin. Medium was changed every three days and experiments were performed after seven days as soon as a confluency of >95% was reached. Organoids were stimulated for 6 h at 37°C with 5 µg mL⁻¹ human recombinant S100A8, S100A9 or S100A8/A9.

Cytokine quantification by enzyme-linked immunosorbent assay in culture supernatant

Extracellular proteins were quantified with enzyme-linked immunosorbent assays (ELISA) or Bio-Plex. Supernatants from human T cells (after 48 h of incubation) were collected, centrifuged for 5 min at 300 g and stored at -20°C. Following Bio-Plex Kits were used for human T cells: Bio-Plex Pro Reagent Kit (Bio-Rad, 171304090M), Bio-Plex Pro HuCSP Standards (Bio-Rad, 12007919), Bio-Plex Pro Human Cytokine IL-17A (Bio-Rad, 171B5014M), Bio-Plex Pro Human Cytokine IFN-γ (Bio-Rad, 171B5019M), Bio-Plex Pro Human Cytokine TNF α (Bio-Rad, 171B5026M).

Immunoblot

Proteins were isolated from MODE-K IECs or human CD8⁺ T cells using M-PER Protein Extraction Reagent (Thermo Fisher Scientific, 78501) containing 1x EDTA and 1x protease and phosphatase

inhibitors (Thermo Fisher Scientific, 78442). Extraction was performed according to manufacturer's instructions and protein quantity was determined by Bradford Assay (Bio-Rad Laboratories, 5000006). Equal amounts of protein were denatured in Laemmli Buffer for 5 min at 95°C and loaded to SDS-PAGE. Proteins were then transferred to a polyvinylidene fluoride membrane (GE HealthCare, GE10600023). Blots were blocked in 5% skim milk and primary antibody was incubated overnight at 4°C. Proteins were visualized using HRP-conjugated secondary antibodies (CST, 7074) and ECL Select Western Blotting Detection Reagent (Amersham, RPN2235). Densitometry of immunoblots was performed in Image Lab. Following antibodies were used: GAPDH (Cell Signaling, 2118), IKK α (3G12)(Cell Signaling, 11930), IKK β (D30C6)(Cell Signaling, 8943), NF- κ B p65 (Cell Signaling, D14E12) XP® (Cell Signaling, 8242), Phospho-IKK α / β (Ser176/180)(16A6)(Cell Signaling, 2697), Phospho-NF- κ B p65 (Ser536)(93H1)(Cell Signaling, 3033), STAT3 (79D7)(Cell Signaling, 4904), Phospho-STAT3 (Tyr705)(D3A7) XP® (Cell Signaling, 9145), S100A8 (abcam, ab92331), S100A9 (Cell Signaling, 72590).

Immunohistochemistry

Immunohistochemistry was performed using standard protocols^{1,5}.

Immunofluorescence

Sections were deparaffinized using xylene and rehydrated in descending-gradient ethanol. Heat-mediated antigen retrieval was performed in a steamer by incubating the samples in citrate buffer (Vector Laboratories, H-3300) for 20 min. Slides were washed, blocked (Protein Block, serum-free, Dako, X0909) for 30 min at RT and incubated with primary antibody dissolved in REAL Ab Diluent (Dako, S2022) overnight at 4°C. Sections were washed with PBS three times for 5 min and incubated with Alexa Fluor 488 secondary antibody for 1 h at RT. Slides were washed and mounted with Prolong Diamond Antifade Mountant including DAPI staining (Invitrogen, P36962). Imaging was performed with an Axio Observer Z1 confocal microscope (Carl Zeiss) and ImageJ was used for analysis.

Following antibodies were used: S100A8 (1:1000) (abcam, ab92331), S100A9 (1:250) (abcam, ab92507), AlexaFluor 488 Donkey anti-Rabbit IgG (Invitrogen, A21206).

Single-cell RNA Sequencing

Monolayer organoid cultures were washed with pre-warmed PBS and incubated with 200 µl of freshly prepared dissociation reagent (TrypLE™ Express Enzyme (ThermoFisher Scientific, 12604013) mixed in a ratio of 1:1 with Accutase (Sigma Aldrich, A6964) containing DNase II) for 15 min at 37°C. Organoid fragments were resuspended thoroughly and the reaction was halted by adding 200 µl of DMEM/F-12 medium containing 10% FCS (Biochrome, S0115). Cell suspensions were centrifuged for 5 min at 200 g and 4°C. Pellets were resuspended in 600 µl of dissociation reagent and incubated for 6 min at 37°C. Reactions were stopped by adding 600 µl of DMEM/F-12 medium containing 10% FCS and samples were centrifuged for 5 min at 200 g and 4°C. To further break down cell bonds, pellets were resuspended in 600 µl trypsin-EDTA (0.05%) containing DNase II for 2 min at 37°C. Suspensions were mixed with 600 µl of DMEM/F-12 medium containing 10% FCS and centrifuged for 5 min at 200 g and 4°C. Dead cells were removed according to manufacturer's instructions (Miltenyi Biotec, Dead Cell Removal Kit, 130-090-101). Briefly, pellets were dissolved in 100 µl of Micro Beads Solution and incubated for 15 min at RT. Suspensions were then separated over MACS Columns (Miltenyi Biotec) in the magnetic field of a MACS Separator (Miltenyi Biotec). Dead cells were retained in the column, while the viable cell fraction was centrifuged for 5 min at 200 g and 4°C. Pellets were dissolved in 100 µl ice-cold PBS containing 0.04% BSA. Single-cell suspensions were submitted to the Medical University of Innsbruck MultiOmics Sequencing Core facility for quality control, counting, and generation of single-cell transcriptome libraries applying the Chromium Controller and the Chromium Automated Single-Cell 3' Reagent Kits User Guide (v3.1) chemistry and protocol from 10x Genomics and targeting 8000-10000 cells per sample. The resulting libraries were sequenced with Illumina NovaSeq technology aiming for a minimum of 20.000 read pairs per targeted cell.

Bulk RNA sequencing of CD8⁺ T cells

After stimulation with human S100A8 (10 µg mL⁻¹), human S100A9 (10 µg mL⁻¹), human S100A8/A9 (10 µg mL⁻¹) or vehicle at 37°C for 4 h, cells were harvested and centrifuged for 5 min at 300 g and 4°C. Medium was discarded and cells were washed once with PBS for 5 min at 300 g and 4°C. RNA isolation was performed according to manufacturer's instructions using an RNeasy Mini Kit (Qiagen, 74104). RNA was immediately stored at -80°C until library preparation. Purified total RNA was submitted to transcriptome analysis at the Medical University of Innsbruck MultiOmics Sequencing Core for the purpose of gene-expression profiling using the QuantSeq 3' mRNA-Seq Library Prep method (Lexogen, Vienna Biocenter). Quality-validated, barcoded libraries were multiplexed and sequenced using Illumina NovaSeq technology.

Bioinformatics analysis

Single-cell RNA sequencing data analysis: 10x fastq sequencing files were processed with the Cell Ranger v7.1.0 (10x Genomics) using the nf-core scRNA-seq pipeline v2.4.1⁶ with the GRCh38 reference genome and GENCODE v44 annotations. The raw count matrices were loaded into AnnData and further processed with scverse tools⁷. Ambient RNA was removed using scAR as implemented in scvi-tools⁸. Quality control was performed on the denoised counts using scanpy⁹, retaining cells with (1) >10000 transcripts, (2) >2000 genes, and (3) <35% mitochondrial transcripts. The 1500 most highly variable genes (HVGs) were selected using scanpy's "highly_variable_genes" function with the options flavor = "seurat_v3" and batch_key = "sample". Cell transcriptomes were embedded into a batch-corrected low-dimensional latent space using scVI^{8,10}, treating each sample as a separate batch. Doublets were identified and removed using SOLO¹¹ as implemented in scvi-tools⁸. The neighborhood graph and uniform manifold approximation and projection (UMAP) embedding¹² were computed based on the scVI latent space. Cell types were annotated based on unsupervised clustering with the Leiden algorithm¹³ and known marker genes^{14,15}. We used DESeq2¹⁶ on pseudo-bulk samples for differential gene expression testing, which has been demonstrated to perform well and properly correct for false discoveries¹⁷. For each cell type and sample we summed up transcript counts for each gene that is expressed in at least 5% of cells using decoupler-py¹⁸. P values were adjusted for multiple hypothesis

testing with independent hypothesis weighting (IHW)¹⁹. Pathway activity analysis was performed with PROGENy²⁰. The t-statistics were computed using a multivariate linear model (mlm) as implemented in decoupler-py and the p-values were adjusted for false-discovery rate (FDR). As input, we used test statistics from the DESeq2 analysis ("stat" column). Bulk RNA sequencing data analysis: We used the nf-core/rnaseq (version 3.12.0) pipeline to align the raw reads to the human genome (GRCh38) with STAR and to assess the read counts on the gene models from GENCODE, version 43, with Salmon^{6,21,22}. We ran the pipeline with the default parameters except for generating the STAR index, where we used the '--sjdbOverhang 200' parameter, and the gene quantification with Salmon, where we set the parameter '--noLengthCorrection', which accounts for the Lexogen 3' QuantSeq RNA sequencing library. Differentially expressed genes between S100A8, S100A9, S100A8/A9 and paired control samples were calculated using DESeq2 (version 1.38.1) using a fold change threshold of 1.5 and a FDR of 0.1 after Independent Hypothesis Weighting (IHW)¹⁶.

For *pathway activity analysis* we used the R decoupleR¹⁸ package and PROGENy²⁰ and applied a multivariate linear model to infer pathway activity scores from differential gene expression using the 'stat' statistic from DESeq2 results. We plotted the resulting pathway activity scores as sorted (high to low) heatmap and marked significant enrichment scores (p value <.01). The androgen and estrogen pathways, neither of which was significant or relevant in this context, were removed from the plot.

Bulk RNA sequencing analysis of the IBDome cohort

RNA-sequencing samples were processed using the nf-core RNA-seq pipeline (version 3.4)⁶. In brief, sequencing reads were aligned to the human reference genome (hg38/GRCh38) using STAR (version 2.7.7a)²¹ with GENCODE v33 annotations. Quantification of read counts and transcripts per million (TPM) was performed using Salmon²².

Subsequent data analyses were conducted in R (version 4.2.3). Visualization of the results was performed using the ggplot2 (version 3.5.1) packages. Pearson correlation coefficients were calculated and displayed in scatter plots using the ggpubr package (version 0.6.0), with statistical significance determined by a p-adjusted cutoff of 0.05.

Statistical analysis

The proportions of patients with detectable S100A8 and S100A9 are presented together with 95% Clopper-Pearson confidence intervals. To assess the association between detectable S100A8 and S100A9 and active disease, logistic regression models were used without adjustment, adjusted for age and sex, and adjusted for age, sex, and type of disease (CD vs. UC). We took into account that data stemmed from two different cohorts by including cohort as an additional covariate in all models. Data are expressed as mean \pm standard error of the mean (SEM), unless otherwise stated. For each experiment sample size (n) is indicated in the figure legend. GraphPad Prism 10 and Stata 15.1 MP was used for statistical analysis. Grubbs test was used for outlier testing. Statistical significance was assessed with an unpaired two-tailed Student's T test, a Mann-Whitney U test, a one-way ANOVA with Bonferroni correction or a Kruskal-Wallis test with Dunn's correction (as appropriate and stated in the figure legends), and was assumed at $*P < .05$, $**P < .01$, $***P < .001$, $****P < .0001$.

Supplemental References

- 1 Schwarzler, J. *et al.* PUFA-Induced Metabolic Enteritis as a Fuel for Crohn's Disease. *Gastroenterology* **162**, 1690-1704 (2022). <https://doi.org/10.1053/j.gastro.2022.01.004>
- 2 Adolph, T. E. *et al.* Paneth cells as a site of origin for intestinal inflammation. *Nature* **503**, 272-276 (2013). <https://doi.org/10.1038/nature12599>
- 3 Martini, G. R. *et al.* Selection of cross-reactive T cells by commensal and food-derived yeasts drives cytotoxic T(H)1 cell responses in Crohn's disease. *Nat Med* **29**, 2602-2614 (2023). <https://doi.org/10.1038/s41591-023-02556-5>
- 4 Bacher, P. *et al.* Human Anti-fungal Th17 Immunity and Pathology Rely on Cross-Reactivity against *Candida albicans*. *Cell* **176**, 1340-1355 e1315 (2019). <https://doi.org/10.1016/j.cell.2019.01.041>
- 5 Mayr, L. *et al.* Dietary lipids fuel GPX4-restricted enteritis resembling Crohn's disease. *Nat Commun* **11**, 1775 (2020). <https://doi.org/10.1038/s41467-020-15646-6>
- 6 Ewels, P. A. *et al.* The nf-core framework for community-curated bioinformatics pipelines. *Nat Biotechnol* **38**, 276-278 (2020). <https://doi.org/10.1038/s41587-020-0439-x>
- 7 Virshup, I. *et al.* The scverse project provides a computational ecosystem for single-cell omics data analysis. *Nat Biotechnol* **41**, 604-606 (2023). <https://doi.org/10.1038/s41587-023-01733-8>
- 8 Gayoso, A. *et al.* A Python library for probabilistic analysis of single-cell omics data. *Nat Biotechnol* **40**, 163-166 (2022). <https://doi.org/10.1038/s41587-021-01206-w>
- 9 Wolf, F. A., Angerer, P. & Theis, F. J. SCANPY: large-scale single-cell gene expression data analysis. *Genome Biol* **19**, 15 (2018). <https://doi.org/10.1186/s13059-017-1382-0>
- 10 Xu, C. *et al.* Probabilistic harmonization and annotation of single-cell transcriptomics data with deep generative models. *Mol Syst Biol* **17**, e9620 (2021). <https://doi.org/10.15252/msb.20209620>
- 11 Bernstein, N. J. *et al.* Solo: Doublet Identification in Single-Cell RNA-Seq via Semi-Supervised Deep Learning. *Cell Syst* **11**, 95-101 e105 (2020). <https://doi.org/10.1016/j.cels.2020.05.010>
- 12 Becht, E. *et al.* Dimensionality reduction for visualizing single-cell data using UMAP. *Nat Biotechnol* (2018). <https://doi.org/10.1038/nbt.4314>
- 13 Traag, V. A., Waltman, L. & van Eck, N. J. From Louvain to Leiden: guaranteeing well-connected communities. *Sci Rep* **9**, 5233 (2019). <https://doi.org/10.1038/s41598-019-41695-z>
- 14 Elmentaite, R. *et al.* Cells of the human intestinal tract mapped across space and time. *Nature* **597**, 250-255 (2021). <https://doi.org/10.1038/s41586-021-03852-1>
- 15 Parikh, K. *et al.* Colonic epithelial cell diversity in health and inflammatory bowel disease. *Nature* **567**, 49-55 (2019). <https://doi.org/10.1038/s41586-019-0992-y>
- 16 Love, M. I., Huber, W. & Anders, S. Moderated estimation of fold change and dispersion for RNA-seq data with DESeq2. *Genome Biol* **15**, 550 (2014). <https://doi.org/10.1186/s13059-014-0550-8>
- 17 Squair, J. W. *et al.* Confronting false discoveries in single-cell differential expression. *Nat Commun* **12**, 5692 (2021). <https://doi.org/10.1038/s41467-021-25960-2>
- 18 Badia, I. M. P. *et al.* decoupleR: ensemble of computational methods to infer biological activities from omics data. *Bioinform Adv* **2**, vbac016 (2022). <https://doi.org/10.1093/bioadv/vbac016>
- 19 Ignatiadis, N., Klaus, B., Zaugg, J. B. & Huber, W. Data-driven hypothesis weighting increases detection power in genome-scale multiple testing. *Nat Methods* **13**, 577-580 (2016). <https://doi.org/10.1038/nmeth.3885>

- 20 Schubert, M. *et al.* Perturbation-response genes reveal signaling footprints in cancer gene expression. *Nat Commun* **9**, 20 (2018). <https://doi.org/10.1038/s41467-017-02391-6>
- 21 Dobin, A. *et al.* STAR: ultrafast universal RNA-seq aligner. *Bioinformatics* **29**, 15-21 (2013). <https://doi.org/10.1093/bioinformatics/bts635>
- 22 Patro, R., Duggal, G., Love, M. I., Irizarry, R. A. & Kingsford, C. Salmon provides fast and bias-aware quantification of transcript expression. *Nat Methods* **14**, 417-419 (2017). <https://doi.org/10.1038/nmeth.4197>

Supplementary Tables

Tables

Supplementary Table 1. Characteristics of the IBDome cohort.

Characteristic	CD	UC	non-IBD	total
No. of samples	235	125	54	414
Female sex - no. (%)	126 (54)	57 (46)	28 (52)	211 (51)
Age at sampling (years) - mean (SD)	38 (14)	42 (16)	56 (17)	42 (16)
BMI at sampling - mean (SD)	25 (5)	26(5)	-	25 (5)
disease localization				
L1: terminal ileum (%)	91 (39)	-	-	-
L2: colon (%)	12 (5)	-	-	-
L3: ileocolon (%)	112 (48)	-	-	-
E1: proctitis (%)	-	7 (6)	-	-
E2: left sided colitis (%)	-	42 (34)	-	-
E3: extensive colitis (%)	-	55 (44)	-	-
disease activity scores				
SES-CD - mean (SD)	5.0 (8.9)	-	0 (0)	-
UCEIS - mean (SD)	-	2.1 (2.5)	0 (0)	-
HBI - mean (SD)	3.2 (3.3)	-	-	-
PMS - mean (SD)	-	1.45 (2.38)	-	-
on treatment*				
Biologics - no. (%)	117 (50)	33 (26)	0 (0)	150 (36)
Conventional therapies - no. (%)	40 (17)	37 (30)	2 (4)	79 (19)
Small molecules - no. (%)	0 (0)	3 (2)	0 (0)	3 (1)
Characteristic	CD	UC	non-IBD	total
No. of patients	152	94	36	282
Female sex - no. (%)	78 (51)	44 (47)	18 (50)	140 (50)
Smoking (%)	27 (18)	5 (5)	2 (6)	34 (12)
previous or ongoing treatment**				
Biologics - no. (%)	108 (71)	47 (50)	0 (0)	155 (55)
Conventional therapies - no. (%)	99 (65)	52 (55)	3 (8)	154 (55)
Small molecules - no. (%)	1 (1)	9 (10)	0 (0)	10 (4)
Probiotics - no. (%)	0 (0)	3 (3)	2 (6)	5 (2)
Non-IBD specific therapies - no. (%)	1 (1)	4 (4)	0 (0)	5 (2)

* Biologics comprise Adalimumab, Golimumab, Infliximab, Ustekinumab, and Vedolizumab; Conventional therapies comprise 5ASA, AZA, Budesonide, Ciclosporin, MTX, Prednisolone, and Sulfasalazine; Small molecules comprise Filgotinib and Tofacitinib;

** Biologics comprise Adalimumab, Golimumab, Infliximab, Risankizumab, Ustekinumab, and Vedolizumab; Conventional therapies comprise 5ASA, 6-MP, AZA, Budesonide, Ciclosporin, Hydrocortisone acetate, MTX, Prednisolone, Sulfasalazine, and Tacrolimus; Small molecules comprise Filgotinib and Tofacitinib; Probiotics comprise E.coli Nissle; and non IBD therapies comprise Ursodeoxycholic acid. Abbreviations: CD, Crohn's disease; UC, Ulcerative colitis; SD, standard deviation; BMI, body mass index; SES-CD, Simple Endoscopic Score for Crohn's Disease; UCEIS, Ulcerative Colitis Endoscopic Index of Severity; HBI, Harvey-Bradshaw Index for Crohn's Disease; PMS, Partial Mayo Score; 5ASA, 5-aminosalicylic acid; AZA, azathioprine; MTX, methotrexate; 6-MP, 6-mercaptopurine.

Supplementary Table 2. Patient characteristics of the IBD cohorts from Innsbruck (Austria) and Groningen (The Netherlands).

Characteristic	Groningen	Innsbruck	Total
Number of patients	316	223	539
Age (years) - mean (SD)	43 (15)	42 (15)	43 (15)
Female sex - no. (%)	188 (59)	113 (51)	301 (56)
CD - no. (%)	184 (58)	154 (69)	338 (63)
Body mass index (kg/m ²) - mean (SD)	25 (5)	24 (4)	25 (5)
Calprotectin detectable - no. (%)			
Patients with CD	130 (71)	141 (92)	271 (80)
Patients with UC	88 (67)	54 (78)	142 (71)
All patients	218 (69)	195 (87)	413 (77)
Calprotectin >150 µg/g - no. (%)			
Patients with CD	36 (20)	68 (44)	104 (31)
Patients with UC	41 (31)	35 (51)	76 (38)
All patients	77 (24)	103 (46)	180 (33)
S100A8 detectable - no. (%)			
Patients with CD	82 (45)	61 (40)	143 (42)
Patients with UC	78 (59)	27 (39)	105 (52)
All patients	160 (51)	88 (39)	248 (46)
S100A9 detectable - no. (%)			
Patients with CD	40 (22)	9 (6)	49 (14)
Patients with UC	31 (23)	3 (4)	34 (17)
All patients	71 (22)	12 (5)	83 (15)
Clinical disease activity - no. (%)*	83 (27)	96 (43)	179 (34)
Calprotectin >150 µg/g	28 (37)	76 (75)	104 (58)
Calprotectin ≤150 µg/g	55 (23)	20 (17)	75 (21)

*Active disease was defined by clinical activity indices available in 534 of 539 patients (99.1%): In the Innsbruck cohort a Crohn's Disease Activity Index >150 among CD patients and a partial Mayo score ≥2 among UC patients indicated clinical disease activity. In the Groningen cohort a Harvey-Bradshaw Index ≥5 among CD patients and an SSCAI score ≥3 among UC patients indicated clinical disease activity. Abbreviations: CD, Crohn's disease; UC, ulcerative colitis.

Supplementary Table 3. Relation of disease localization with fecal dimer detection.

	Montreal L1*	Montreal L2	Montreal L3	Test	P-value
All CD patients					
	N=79	N=60	N=189		
Fecal calprotectin (µg/g)	53.5 (0.0-179.2)	52.0 (18.3-161.1)	85.7 (25.5-198.2)	Kruskal-Wallis	0.14
Detectable S100A8- no.(%)				Chi-square	0.80
No	43 (54.4%)	35 (58.3%)	111 (58.7%)		
Yes	36 (45.6%)	25 (41.7%)	78 (41.3%)		
Detectable S100A9- no.(%)				Chi-square	0.79
No	69 (87.3%)	53 (88.3%)	161 (85.2%)		
Yes	10 (12.7%)	7 (11.7%)	28 (14.8%)		
Patients with calprotectin ≤150 µg/g stool					
	N=58	N=43	N=128		
Fecal calprotectin (µg/g)	30.9 (0.0-62.9)	29.1 (0.0-56.0)	44.9 (16.1-87.2)	Kruskal-Wallis	0.056
Detectable S100A8- no.(%)				Chi-square	0.85
No	32 (55.2%)	26 (60.5%)	75 (58.6%)		
Yes	26 (44.8%)	17 (39.5%)	53 (41.4%)		
Detectable S100A9- no.(%)				Chi-square	0.72
No	51 (87.9%)	38 (88.4%)	108 (84.4%)		
Yes	7 (12.1%)	5 (11.6%)	20 (15.6%)		

* Montreal L1 is defined as ileal disease, Montreal L2 is defined as colonic disease and Montreal L3 is defined as ileocolonic disease. Abbreviations: CD, Crohn's disease.

Supplementary Table 4. Relation of smoking status, body mass index, C-reactive protein and hemoglobin concentration with fecal dimer detection.

Patients with calprotectin ≤ 150 $\mu\text{g/g}$ stool				
S100A8 detectable	No	Yes	Test	P-value
	N=192	N=167		
Smoking status- no. (%)			Chi-square	0.20
Current	40 (21.3%)	27 (16.6%)		
Ex	48 (25.5%)	55 (33.7%)		
Never	100 (53.2%)	81 (49.7%)		
Body mass index	25.0 \pm 4.4	24.7 \pm 4.5	independent t test	0.56
C-reactive protein (mg/L)	1.10 (0.00-3.50)	1.30 (0.00-5.20)	Wilcoxon rank-sum	0.49
Hemoglobin (g/dL)	14.1 \pm 1.6	13.6 \pm 1.5	independent t test	0.080
S100A9 detectable	No	Yes	Test	P-value
	N=303	N=56		
Smoking status- no. (%)			Chi-square	0.014
Current	56 (19.0%)	11 (19.6%)		
Ex	78 (26.4%)	25 (44.6%)		
Never	161 (54.6%)	20 (35.7%)		
Body mass index	24.7 \pm 4.3	25.6 \pm 5.1	independent t test	0.14
C-reactive protein (mg/L)	1.30 (0.00-3.80)	1.00 (0.00-4.90)	Wilcoxon rank-sum	0.80
Hemoglobin (g/dL)	14.0 \pm 1.6	13.3 \pm 1.0	independent t test	0.37

Supplementary Table 5. Patient characteristics of the adult IBD cohort from Kiel, Germany.

	Active*		Remission	
Number of patients	65		19	
male/female %	66/34		53/47	
Age \pm SD	41.44	17.03	41.28	10.91
BMI \pm SD	25.41	5.91	25.20	4.34
CRP (mg/L) \pm SD	8.68	14.40	3.14	3.83
Hb (g/dL) \pm SD	13.05	2.00	13.44	1.57
CD/UC %	23/77		63/37	
CDAI (CD) \pm SD	122.40	82.66	141.58	80.29
Partial Mayo (UC) \pm SD	2.98	2.63	1.00	1.07
SES-CD (CD) \pm SD	8.07	4.27	0.58	0.76
Endo Mayo (UC) \pm SD	1.76	0.76	0	0
Median calprotectin in colonic aspirate (μ g/mL)	0.41		0.41	

*Active disease was defined by endoscopic disease activity (SES-CD>2 or Endoscopic Mayo Score >0). Abbreviations: BMI, body mass index; CRP, C-reactive protein; Hb, hemoglobin; CD, Crohn's disease; UC, ulcerative colitis; CDAI, Crohn's disease activity index; Partial Mayo, Partial Mayo Scoring Index; SES-CD, Simple Endoscopic Score; Endo Mayo, Endoscopic Mayo Scoring Index.

Supplementary Table 6. Human protein interaction partners of S100A8 in stool from active IBD patients.

S100A8 Co-IP	Abundance Ratio: (S100A8-IP) / (control-IP)	Abundance Ratio P-Value: (S100A8-IP) / (control-IP)	Abundance Ratio Adj. P- Value: (S100A8-IP) / (control-IP)
Matrix metalloproteinase-15 OS=Homo sapiens OX=9606 GN=MMP15 PE=1 SV=1	1000	1.00E-17	3.88E-16
Galectin-4 OS=Homo sapiens OX=9606 GN=LGALS4 PE=1 SV=1	1000	1.00E-17	3.88E-16
ATP synthase subunit beta, mitochondrial OS=Homo sapiens OX=9606 GN=ATP5F1B PE=1 SV=3	1000	1.00E-17	3.88E-16
Disco-interacting protein 2 homolog B OS=Homo sapiens OX=9606 GN=DIP2B PE=1 SV=3	1000	1.00E-17	3.88E-16
Mesencephalic astrocyte-derived neurotrophic factor OS=Homo sapiens OX=9606 GN=MANF PE=1 SV=3	913.72	1.00E-17	3.88E-16
Immunoglobulin heavy constant gamma 4 OS=Homo sapiens OX=9606 GN=IGHG4 PE=1 SV=1	139.92	1.00E-17	3.88E-16
Triple functional domain protein OS=Homo sapiens OX=9606 GN=TRIO PE=1 SV=2	102.96	1.00E-17	3.88E-16
Putative methyltransferase NSUN5C OS=Homo sapiens OX=9606 GN=NSUN5P2 PE=5 SV=2	80.71	1.00E-17	3.88E-16
Immunoglobulin kappa variable 4-1 OS=Homo sapiens OX=9606 GN=IGKV4-1 PE=1 SV=1	48.63	4.88E-15	1.63E-13
A disintegrin and metalloproteinase with thrombospondin motifs 17 OS=Homo sapiens OX=9606 GN=ADAMTS17 PE=2 SV=2	35.41	7.02E-13	2.18E-11
Semaphorin-3A OS=Homo sapiens OX=9606 GN=SEMA3A PE=1 SV=1	32.99	2.01E-12	5.86E-11
Inhibitor of Bruton tyrosine kinase OS=Homo sapiens OX=9606 GN=IBTK PE=1 SV=3	21.51	7.40E-10	1.86E-08
NACHT, LRR and PYD domains- containing protein 1 OS=Homo sapiens OX=9606 GN=NLRP1 PE=1 SV=1	20.32	1.53E-09	3.66E-08
Immunoglobulin heavy variable 3-43 OS=Homo sapiens OX=9606 GN=IGHV3-43 PE=3 SV=1	18.05	6.68E-09	1.45E-07
Protein S100-A9 OS=Homo sapiens OX=9606 GN=S100A9 PE=1 SV=1	15.20	5.13E-08	1.04E-06

Protein S100-A8 OS=Homo sapiens OX=9606 GN=S100A8 PE=1 SV=1	14.20	1.12E-07	2.22E-06
Immunoglobulin kappa variable 1-9 OS=Homo sapiens OX=9606 GN=IGKV1-9 PE=3 SV=1	13.50	1.96E-07	3.72E-06
Chymotrypsin-like elastase family member 2A OS=Homo sapiens OX=9606 GN=CELA2A PE=1 SV=1	11.25	1.37E-06	2.45E-05
Immunoglobulin heavy constant gamma 3 OS=Homo sapiens OX=9606 GN=IGHG3 PE=1 SV=2	11.14	1.51E-06	2.66E-05
DNA primase large subunit OS=Homo sapiens OX=9606 GN=PRIM2 PE=1 SV=2	11.01	1.71E-06	2.95E-05
Creatine kinase U-type, mitochondrial OS=Homo sapiens OX=9606 GN=CKMT1B PE=1 SV=1	10.35	3.19E-06	5.31E-05
ADP-ribosylation factor 3 OS=Homo sapiens OX=9606 GN=ARF3 PE=1 SV=2	8.97	1.27E-05	1.97E-04
Immunoglobulin kappa variable 1D- 39 OS=Homo sapiens OX=9606 GN=IGKV1D-39 PE=3 SV=2	7.48	6.48E-05	9.90E-04
Carboxypeptidase A2 OS=Homo sapiens OX=9606 GN=CPA2 PE=1 SV=3	6.62	1.81E-04	2.68E-03
Cofilin-1 OS=Homo sapiens OX=9606 GN=CFL1 PE=1 SV=3	6.22	2.98E-04	4.34E-03
Zymogen granule membrane protein 16 OS=Homo sapiens OX=9606 GN=ZG16 PE=1 SV=2	5.43	8.45E-04	1.09E-02
Protein S100-A12 OS=Homo sapiens OX=9606 GN=S100A12 PE=1 SV=2	5.22	1.13E-03	1.45E-02
Histone H2B type 1-K OS=Homo sapiens OX=9606 GN=HIST1H2BK PE=1 SV=3	4.83	1.95E-03	2.43E-02
Immunoglobulin kappa variable 6D- 21 OS=Homo sapiens OX=9606 GN=IGKV6D-21 PE=3 SV=1	4.77	2.14E-03	2.62E-02
Integrin beta-3 OS=Homo sapiens OX=9606 GN=ITGB3 PE=1 SV=2	4.66	2.51E-03	2.92E-02
Alpha-2-macroglobulin OS=Homo sapiens OX=9606 GN=A2M PE=1 SV=3	4.38	3.75E-03	4.11E-02
Immunoglobulin kappa joining 1 OS=Homo sapiens OX=9606 GN=IGKJ1 PE=4 SV=2	4.29	4.32E-03	4.62E-02

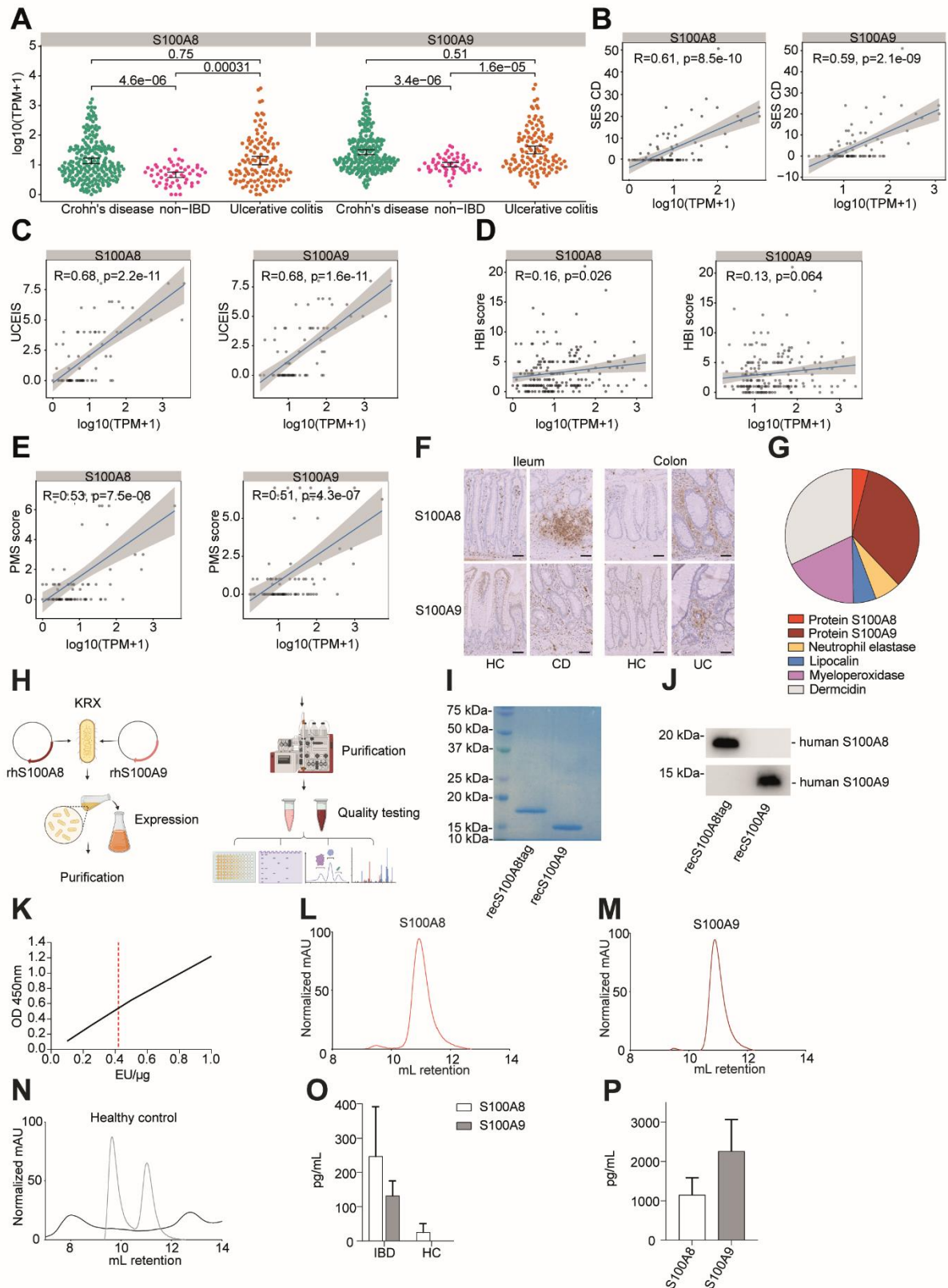
Supplementary Table 7. Human protein interaction partners of S100A9 in stool from active IBD patients.

S100A9 Co-IP	Abundance Ratio: (S100A9-IP) / (control-IP)	Abundance Ratio P-Value: (S100A9-IP) / (control-IP)	Abundance Ratio Adj. P-Value: (S100A9-IP) / (control-IP)
Matrix metalloproteinase-15 OS=Homo sapiens OX=9606 GN=MMP15 PE=1 SV=1	1000	1.00E-17	4.66E-16
CD177 antigen OS=Homo sapiens OX=9606 GN=CD177 PE=1 SV=2	585.84	1.00E-17	4.66E-16
ATP synthase subunit beta, mitochondrial OS=Homo sapiens OX=9606 GN=ATP5F1B PE=1 SV=3	559.69	1.00E-17	4.66E-16
Disco-interacting protein 2 homolog B OS=Homo sapiens OX=9606 GN=DIP2B PE=1 SV=3	156.95	1.00E-17	4.66E-16
Galectin-4 OS=Homo sapiens OX=9606 GN=LGALS4 PE=1 SV=1	90.53	1.00E-17	4.66E-16
Immunoglobulin heavy constant gamma 4 OS=Homo sapiens OX=9606 GN=IGHG4 PE=1 SV=1	20.88	1.00E-17	4.66E-16
Triple functional domain protein OS=Homo sapiens OX=9606 GN=TRIO PE=1 SV=2	20.52	1.00E-17	4.66E-16
Immunoglobulin heavy variable 2-26 OS=Homo sapiens OX=9606 GN=IGHV2-26 PE=3 SV=1	7.65	2.14E-10	9.07E-09
NACHT, LRR and PYD domains- containing protein 1 OS=Homo sapiens OX=9606 GN=NLRP1 PE=1 SV=1	6.22	1.33E-08	4.95E-07
Immunoglobulin heavy constant gamma 3 OS=Homo sapiens OX=9606 GN=IGHG3 PE=1 SV=2	5.48	1.37E-07	4.41E-06
Cilia- and flagella-associated protein 74 OS=Homo sapiens OX=9606 GN=CFAP74 PE=2 SV=3	4.43	4.76E-06	1.35E-04
Protein S100-A9 OS=Homo sapiens OX=9606 GN=S100A9 PE=1 SV=1	3.97	2.38E-05	6.33E-04
Protein S100-A8 OS=Homo sapiens OX=9606 GN=S100A8 PE=1 SV=1	3.95	2.56E-05	6.62E-04
DNA primase large subunit OS=Homo sapiens OX=9606 GN=PRIM2 PE=1 SV=2	3.87	3.43E-05	8.65E-04
Immunoglobulin kappa variable 1-9 OS=Homo sapiens OX=9606 GN=IGKV1-9 PE=3 SV=1	3.43	1.81E-04	4.12E-03
Immunoglobulin kappa variable 1D-8 OS=Homo sapiens OX=9606 GN=IGKV1D-8 PE=3 SV=6	3.17	4.76E-04	1.06E-02

Supplementary Table 8. Mass list table used for spike-in experiments.

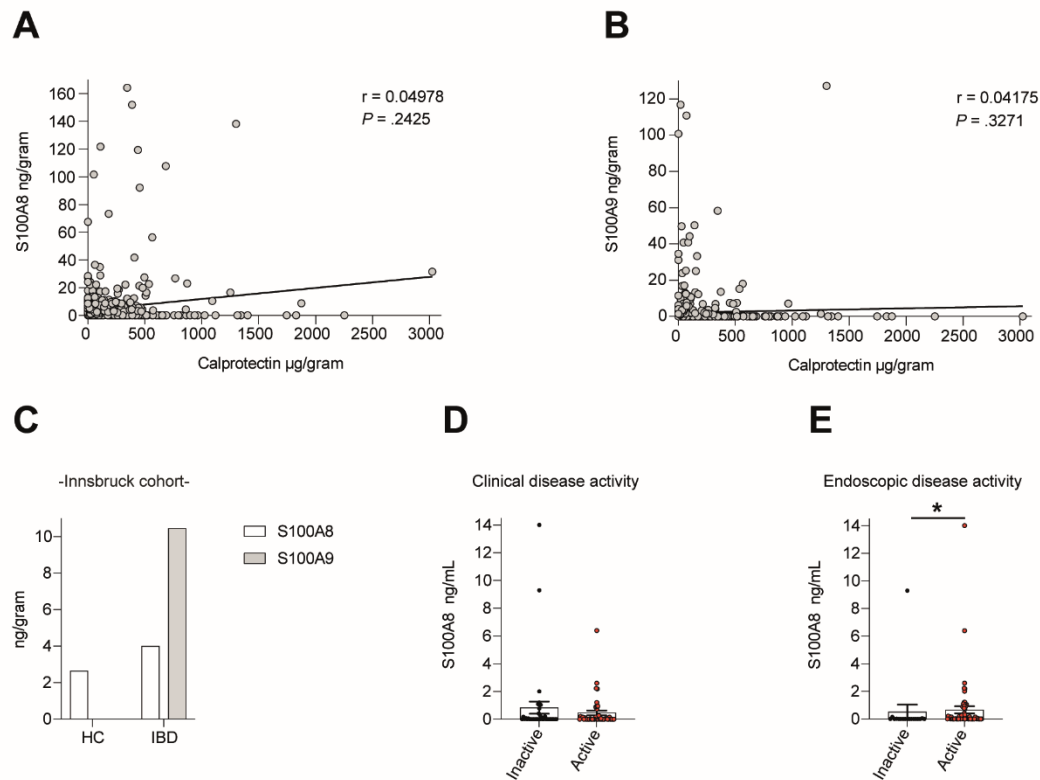
Protein	Peptide Sequence	Modification	Position in Protein	m/z	z	t start (min)	stop (min)	HCD Collision Energy (%)
S100A8	ALNSIIDV YHK		8-18	424,9031	3	12,88	15,88	30
S100A8	ALNSIIDV YHK	Label 13C15N [K18]	8-18	427,5666	3	12,88	15,88	30
S100A8	GNFHAV YR		24-31	482,2436	2	9,11	12,11	33
S100A8	LLETECP QYIR	Carbamido- methyl [C42]	37-47	711,3583	2	12,56	15,56	30
S100A8	KGADVW FK		49-56	475,7584	2	11,18	14,18	33
S100A8	GADVWF K		50-56	411,7109	2	13,01	14,01	30
S100A9	MSQLER	Oxidation [M5]	5-10	390,1894	2	7,99	10,99	30
S100A9	MSQLER		5-10	382,1918	2	8,78	11,78	30
S100A9	NIETIINT FHQYSVK		11-25	602,9843	3	15,12	18,12	30
S100A9	LGHPDTL NQGEFK		26-38	485,9124	3	10,64	13,64	33
S100A9	LGHPDTL NQGEFK	Label 13C15N [K38]	26-38	488,5786	3	10,64	13,64	33
S100A9	DLQNFLK		44-50	439,2425	2	14,28	17,28	30
S100A9	VIEHIME DLDTNA DK		58-72	581,6137	3	13,02	16,02	30
S100A9	VIEHIME DLDTNA DK	Oxidation [M63]	58-72	586,9453	3	11,37	14,37	30
S100A9	LTWASHE K		86-93	486,2511	2	9,17	12,17	30
S100A9	MHEGDE GPGHHH KPGLGEG TP		94-114	544,7461	4	8,5	11,5	30
S100A9	MHEGDE GPGHHH KPGLGEG TP	Oxidation [M9]	94-114	548,7448	4	8,07	11,07	30

Supplementary Figures

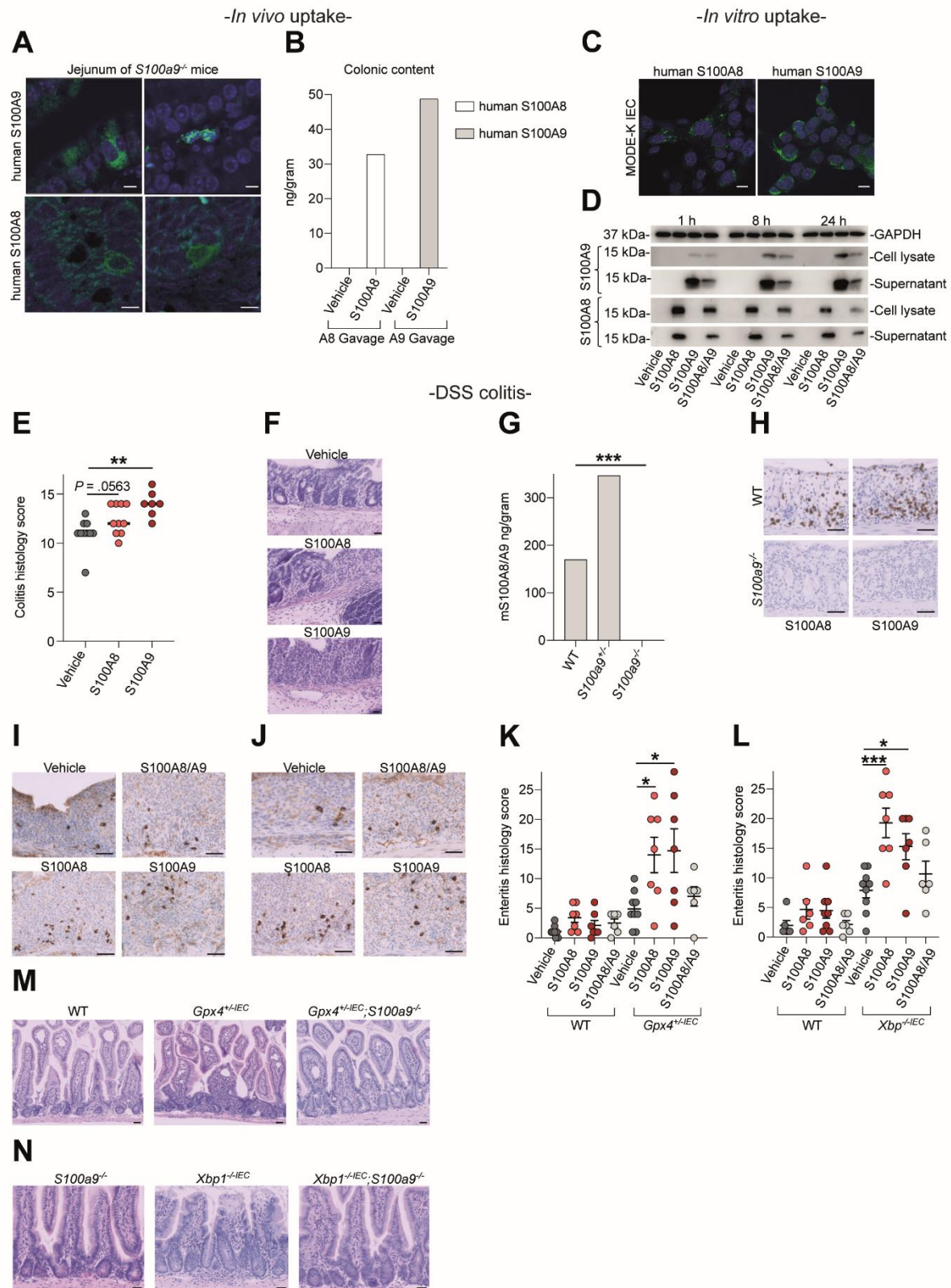


Supplementary Figure 1. Generation of human recombinant S100A8 and S100A9. A. Mucosal expression levels of *S100A8* and *S100A9* in patients with Crohn's disease (green) and Ulcerative Colitis (orange) compared to non-IBD patients (pink) with P-values retrieved with the Wilcoxon-Mann-

Whitney test. **B, C.** Mucosal expression levels of *S100A8* and *S100A9* in patients with **(B)** CD and **(C)** UC correlated with endoscopic disease activity as assessed by Simple Endoscopic Score (SES-CD) and Ulcerative Colitis Endoscopic Index of Severity (UCEIS). **D, E.** Mucosal expression levels of *S100A8* and *S100A9* in patients with **(D)** CD and **(E)** UC correlated with clinical disease activity as assessed by Harvey-Bradshaw Index (HBI) and Partial Mayo Score (PMS). **F.** Representative immunohistochemistry images of *S100A8* and *S100A9* in the ileum of CD patients and colon of UC patients compared to healthy controls (HC). Scale bars, 50 μ m. **G.** Relative proportion of abundant proteins consistently detectable in stool of all IBD patients (CD, n=8; UC n=8) analyzed with LC-MS/MS. **H.** Schematic workflow for the production and purification of human recombinant *S100A8* and *S100A9*. Image was created in <https://BioRender.com>. **I.** Representative Coomassie staining of human recombinant *S100A8* and *S100A9* protein. **J.** Immunoblot of human recombinant *S100A8* and *S100A9* protein. **K.** Representative endotoxin test for human recombinant *S100A8* and *S100A9* (dotted line) depicted in EU per μ g of recombinant protein. **L, M.** Representative size-exclusion chromatography (SEC) spectra of human recombinant *S100A8* (**L**) and *S100A9* (**M**) homodimers. **N.** Representative SEC spectra of stool dissolved in PBS from healthy controls (n=4). Grey spectra are chromatographic peaks of human recombinant calprotectin dimers and tetramers, indicating the SEC fractions containing *S100A8*/*S100A9* dimers in human stool. **O.** Quantification of *S100A8* and *S100A9* concentration in SEC fractions of stool at a size compatible with homo- or heterodimers in IBD patients with a positive ELISA, and healthy controls (HC) (n=8/4). **P.** Quantification of *S100A8* and *S100A9* concentration in SEC fractions of endoscopy washes at a size compatible with homo- or heterodimers in CD and UC patients by ELISA (n=3/3).

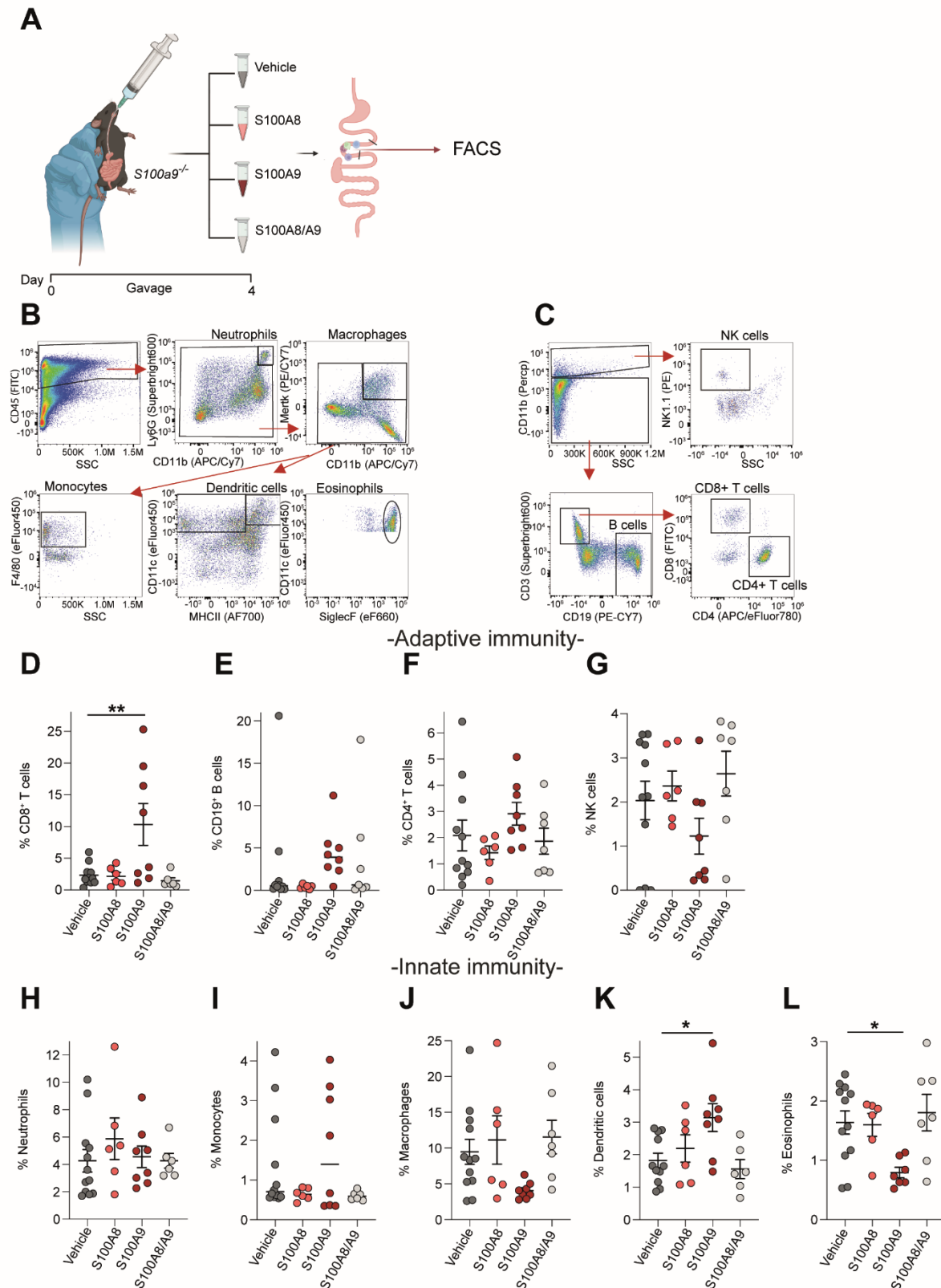


Supplementary Figure 2. Quantification of S100A8 and S100A9 in IBD. **A, B.** Correlation between fecal S100A8 concentration with fecal calprotectin concentration (**A**) and fecal S100A9 concentration with fecal calprotectin concentration (**B**), as assessed by nonparametric Spearman correlation. Each dot represents one patient from the Innsbruck and 1000IBD Groningen cohort (n=539). **C.** Quantification of fecal S100A8 and S100A9 concentration from HC and IBD patients in Innsbruck with a positive ELISA. **D, E.** Quantification of S100A8 concentration in endoscopic aspirates from the colon of IBD patients with calprotectin concentration $\leq 150 \mu\text{g/mL}$ in IBD patients stratified by clinical disease activity (**D**) or endoscopic disease activity (**E**) in a cohort from Kiel, Germany (n=84). * $P < .05$.



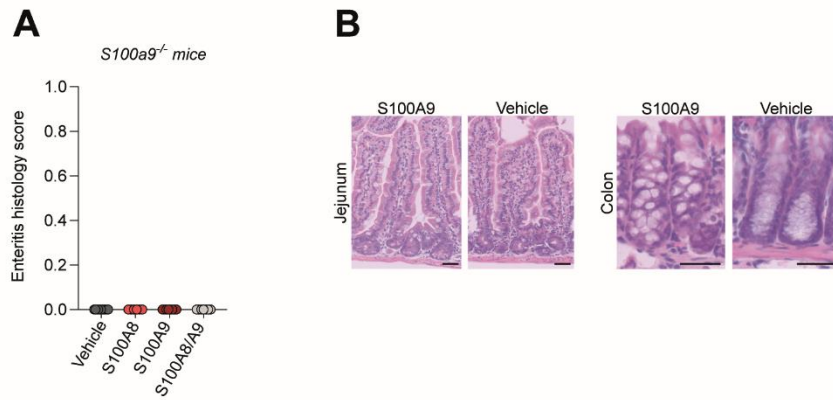
Supplementary Figure 3. Human recombinant S100A8 and S100A9 homodimers promote enteritis and colitis. **A.** Representative confocal images of the small intestine of *S100a9*^{-/-} mice orally gavaged with human recombinant S100A9 or S100A8 (green) for four days. DAPI (blue) indicates nuclei. Scale bars, 10 μ m. **B.** ELISA-based quantification of human S100A8 or human S100A9 in

colonic stool obtained from *S100a9*^{-/-} mice orally gavaged with human recombinant S100A8 or S100A9. **C.** Representative confocal images of MODE-K IECs incubated with human recombinant S100A9 or S100A8 (green) protein. DAPI (blue) indicates nuclei. Scale bars, 5 μ m. **D.** Representative immunoblot of human S100A8 and S100A9 from cell lysates and supernatants of MODE-K IECs stimulated with vehicle, S100A8, S100A9 or the 1:1 mix (calprotectin) for indicated time points after rigorous washing. **E, F.** Colitis histology score of DSS (for 5 days) treated *S100a9*^{-/-} mice after vehicle, human S100A8 or S100A9 gavage for 4 consecutive days (**E**), at day 8 (n=7-11; 8-9 weeks; median shown, Kruskal-Wallis-Test with Dunn's correction) and representative H&E images (**F**). Scale bars, 50 μ m. **G, H.** Confirmation of calprotectin deletion in *S100a9*^{-/-} mice by quantification of calprotectin in stool by ELISA (**G**) and by immunohistochemistry of murine S100A8 and S100A9 (**H**) in the colon of mice exposed to DSS. Scale bars, 100 μ m. **I, J.** Representative immunohistochemistry images of CD4⁺ T cells (**I**) and CD8⁺ T cells (**J**) in the colon of WT mice exposed to DSS and oral gavage of vehicle or human recombinant S100A8, S100A9 or the 1:1 mix (**as in Figure 3A-F**). Scale bars, 100 μ m. **K.** Enteritis histology score of wild-type and *Gpx4*^{+/-IEC} mice fed a PUFA-enriched WD for three months and oral exposure to vehicle or human recombinant S100A8, S100A9 or the 1:1 mix (calprotectin) once daily for the final seven days of the experiment (n=9/7/7/6; 7-8 weeks; mean \pm SEM shown; one-way ANOVA with post-hoc Bonferroni). **L.** Enteritis histology score of WT and *Xbp1*^{-/-IEC} mice fed a PUFA-enriched WD for three months and oral exposure to vehicle or human recombinant S100A8, S100A9 or the 1:1 mix (calprotectin) once daily for the final seven days of the experiment (n=9/7/7/6; 7-8 weeks; mean \pm SEM shown; one-way ANOVA with post-hoc Bonferroni). **M, N.** Representative H&E images of mice scored in Figure 3L (**M**) and in Figure 3M (**N**). Scale bars, 50 μ m. **P* <.05, ***P* <.02, ****P* <.001.

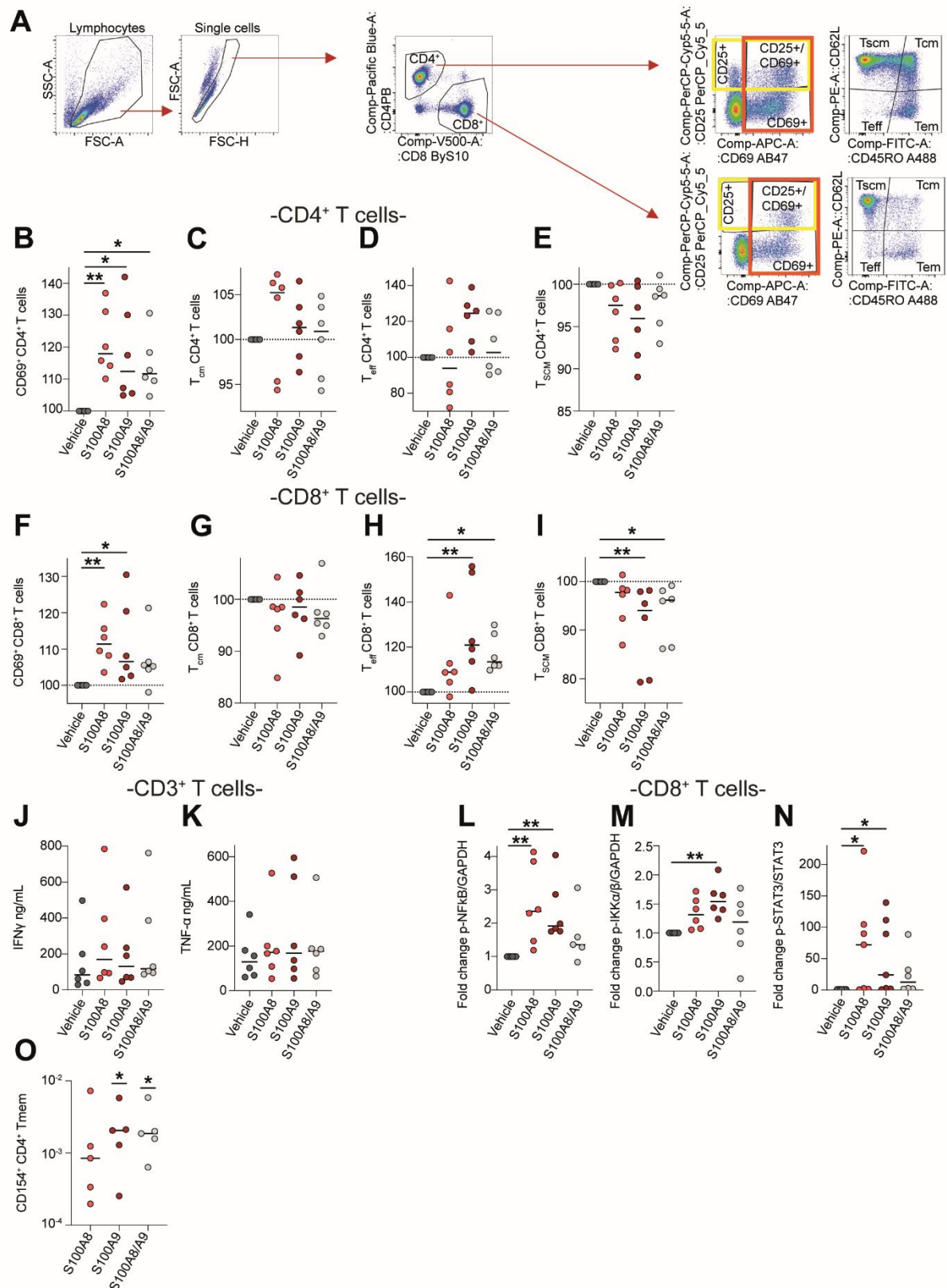


Supplementary Figure 4. Immune phenotyping of mouse gut mucosa after exposure to human S100A8 or S100A9 homodimers. **A.** Schematic illustration of experimental design: *S100a9*^{-/-} mice were orally gavaged with vehicle or 100 µg S100A8 or S100A9 or the 1:1 mix (calprotectin) once daily for four consecutive days. Tissue samples from small intestinal mucosa (jejunum) were used for flow

cytometry phenotyping. Image was created in <https://BioRender.com>. **B.** Flow cytometry gating strategy for single CD45⁺, CD3⁻, CD19⁻, CD49b⁻ and DAPI⁻ innate immune cells present in the lamina propria of the small intestine. **C.** Flow cytometry gating strategy for single CD45⁺, CD11c⁻, F4/80⁻, GR1⁻ and DAPI⁻ adaptive immune cells present in the lamina propria of the small intestine. **D-G.** Quantification of CD8⁺ T cells (**D**), CD19⁺ B cells (**E**), CD4⁺ T cells (**F**) and NK-cells (**G**) in *S100a9*^{-/-} mice after oral gavage with vehicle, S100A8, S100A9 or the 1:1 mix (calprotectin) for four days by flow cytometry (n=11/6/8/7; 7-8 weeks; mean ± SEM shown; one-way ANOVA with post-hoc Bonferroni). **H-L.** Quantification of indicated innate immune cells in *S100a9*^{-/-} mice after oral gavage with vehicle, S100A8, S100A9 or the 1:1 mix (calprotectin) for four days (n=12/6/8/7; 7-8 weeks; mean ± SEM shown; one-way ANOVA with post-hoc Bonferroni). Data is depicted in percent of CD45⁺ single cells. **P* < .05, ***P* < .01.



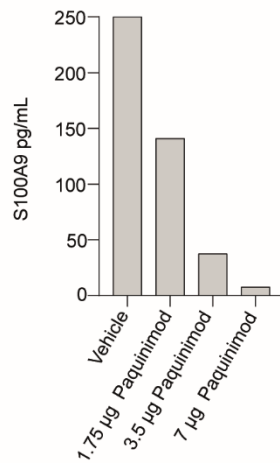
Supplementary Figure 5. S100A8 or S100A9 gavage does not induce gut inflammation. A. Enteritis histology score for *S100a9^{-/-}* mice after oral gavage of vehicle, S100A8, S100A9 or the 1:1 mix (calprotectin) for four days (n=11/6/8/7; 7-8 weeks; median shown). **B.** Representative H&E images of the small intestine and colon of *S100a9^{-/-}* mice after oral gavage with human recombinant S100A9. Scale bars, 50 μ m.



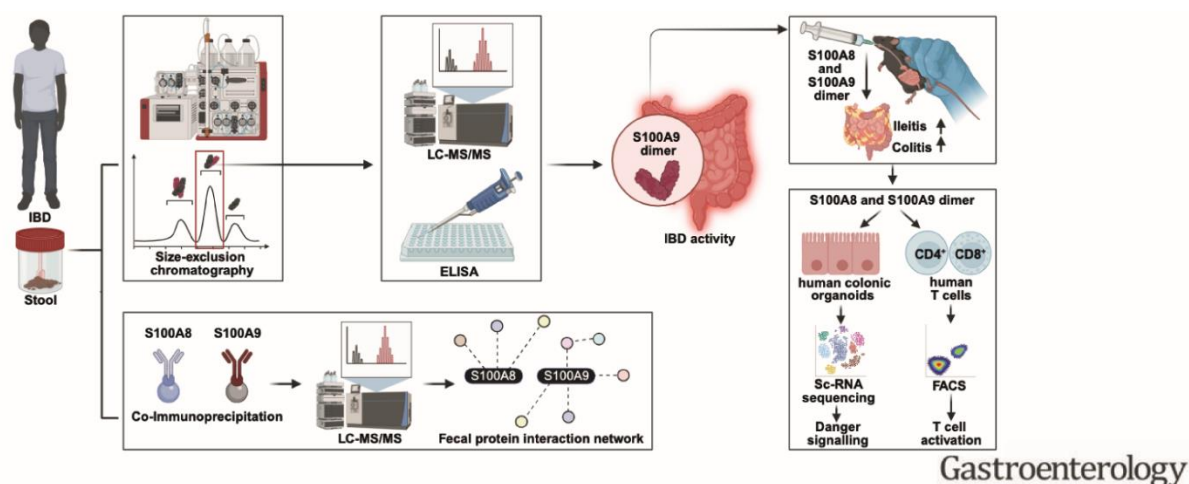
Supplementary Figure 6. Immunophenotyping of human blood-derived CD4⁺ and CD8⁺ T cells after stimulation with human recombinant S100A8 and S100A9 homodimers. The experimental approach is summarized in Figure 5A. **A.** Flow cytometry gating strategy for sorted CD3⁺ T cell that was used to analyze the phenotype of activated CD4⁺ and CD8⁺ T cells. Gating was performed for

following surface markers: CD25, CD69, CD62L, CD45RO. Cell populations were defined as follows: T_{scm} : CD62L⁺/CD45RO⁻, T_{CM} : CD62L⁺/CD45RO⁺, T_{eff} : CD62L⁻/CD45RO⁻. **B.** Quantification of activated CD4⁺ T cells after stimulation with S100A8, S100A9 or the 1:1 mix (calprotectin) for 24 h when compared to vehicle (n=6/6/6/6; Kruskal-Wallis test with Dunn's correction; median shown). **C.** Quantification of central memory CD4⁺ T cells after stimulation with S100A8, S100A9 or the 1:1 mix (calprotectin) for 24 h when compared to vehicle (n=6/6/6/6; Kruskal-Wallis test with Dunn's correction; median shown). **D.** Quantification of effector CD4⁺ T cells after stimulation with S100A8, S100A9 or the 1:1 mix (calprotectin) for 24 h when compared to vehicle (n=6/6/6/6; Kruskal-Wallis test with Dunn's correction; median shown). **E.** Quantification of stem cell-like memory CD4⁺ T cells after stimulation with S100A8, S100A9 or the 1:1 mix (calprotectin) for 24 h when compared to vehicle (n=6/6/6/6; Kruskal-Wallis test with Dunn's correction; median shown). **F.** Quantification of activated CD8⁺ T cells after stimulation with S100A8, S100A9 or the 1:1 mix (calprotectin) for 24 h when compared to vehicle (n=6/6/6/6; Kruskal-Wallis test with Dunn's correction; median shown). **G.** Quantification of central memory CD8⁺ T cells after stimulation with S100A8, S100A9 or the 1:1 mix (calprotectin) for 24 h when compared to vehicle (n=6/6/6/6; Kruskal-Wallis test with Dunn's correction; median shown). **H.** Quantification of effector CD8⁺ T cells after stimulation with S100A8, S100A9 or the 1:1 mix (calprotectin) for 24 h when compared to vehicle (n=6/6/6/6; Kruskal-Wallis test with Dunn's correction; median shown). **I.** Quantification of stem cell-like memory CD8⁺ T cells after stimulation with S100A8, S100A9 or the 1:1 mix (calprotectin) for 24 h when compared to vehicle (n=6/6/6/6; Kruskal-Wallis test with Dunn's correction; median shown). **J.** Quantification of IFN γ concentration in the supernatant of CD3⁺ T cells after stimulation with S100A8, S100A9 or the 1:1 mix (calprotectin) for 48 h when compared to vehicle, determined by Bio-Plex (n=6/6/6/6; Kruskal-Wallis test with Dunn's correction; median shown). **K.** Quantification of TNF- α concentration in the supernatant of CD3⁺ T cells after stimulation with S100A8, S100A9 and S100A8/A9 for 48 h, determined by Bio-Plex (n=6/6/6/6; Kruskal-Wallis test with Dunn's correction; median shown). **L-N.** Quantification of relative phosphorylation of NF- κ B (n=6) (**L**), IKK α/β (n=6) (**M**), and STAT3 (n=7) (**N**) by densitometry of immunoblots from human CD8⁺ T cells stimulated with vehicle, S100A8, S100A9 or the 1:1 mix (calprotectin). **O.** Quantification of antigen-activated CD4⁺ CD154⁺ T cells after stimulation with S100A8, S100A9 or the 1:1 mix (calprotectin). Values are shown relative to vehicle stimulation, as is statistical significance (n=5/5/5/5; Kruskal-Wallis test with Dunn's correction; median shown). * $P < .05$, ** $P < .01$.

A



Supplementary Figure 7. Paquinimod inhibits S100A9 suggested by ELISA. A. Quantification of human recombinant S100A9 homodimers in the presence of increasing concentrations of paquinimod, as determined by ELISA.



Supplementary Figure 8. Graphical Abstract. Stool and endoscopic aspirates from patients with active IBD commonly contain S100A8 and S100A9 dimers, as validated by size-exclusion chromatography coupled with LC-MS/MS and specific ELISA. Fecal S100A9 detection by ELISA associated with clinical and endoscopic disease activity in IBD patients with low CP concentration ($<150\mu\text{g/g}$). Human recombinant S100A8 and S100A9 homodimers worsen experimental enteritis and colitis in mice. Human S100A8 and S100A9 homodimers induce epithelial danger signalling in colonic organoids and enhanced activation of CD4^+ and CD8^+ T cells. In line, adaptive immunity is required for the inflammatory actions of human S100A8 and S100A9 homodimers in the mouse intestine. Moreover, co-immunoprecipitation of S100A8 and S100A9 from stool of patients with IBD coupled with LC-MS/MS identifies the fecal protein interaction network of dimers. Collectively, this study unravels inflammatory actions of S100A8 and S100A9 dimers in IBD which could be used for diagnostic and therapeutic purposes. Image was created in <https://BioRender.com>.